Open access • Journal Article • DOI:10.1016/J.COMPOSITESB.2017.03.010

Exact three-dimensional static analysis of single- and multi-layered plates and shells — Source link

Salvatore Brischetto

Institutions: Polytechnic University of Turin

Published on: 15 Jun 2017 - Composites Part B-engineering (Elsevier)

Topics: Spherical shell, Shell (structure), Finite element method, Curvilinear coordinates and Boundary value problem

Exact three-dimensional static analysis of single- and multi-layered plates and shells

Exact three-dimensional static analysis of single- and multi-layered plates and shells

Salvatore Brischetto*

Abstract

This new work proposes an exact three-dimensional static analysis of plates and shells. One-layered and multilayered isotropic, orthotropic, sandwich and composite structures are investigated in terms of displacements and in-plane and out-of-plane stresses through the thickness direction. Proposed structures are completely simply-supported and a transverse normal load is applied. The proposed method is based on the 3D equilibrium equations written using general orthogonal curvilinear coordinates which are valid for spherical shells. Cylindrical shell, cylinder and plate results are obtained as particular cases of 3D spherical shell equations. All the considered structures are analyzed without any geometrical approximation. The exact solution is possible because of simply-supported boundary conditions and harmonic form for applied loads. The shell solution is based on a layer-wise approach and the second order differential equations are solved using the redouble of variables and the exponential matrix method. A preliminary validation of the model is made using reference results in the literature. Thereafter, the proposed exact 3D shell solution is employed with confidence to provide results for one-layered and multilayered plates, cylinders, cylindrical shell panels and spherical shell panels. All these geometries are analyzed via a unified and general solution, and the obtained results can be used to validate future numerical methods proposed for plates and shells (e.g., the finite element method or the differential quadrature method). Proposed results allow to remark substantial features about the thickness of the structures, their geometry, the zigzag effects of displacements, the interlaminar continuity of displacements and transverse stresses, and boundary loading conditions for stresses.

Keywords: plates and shells; 3D exact solution; layer-wise approach; exponential matrix method; static analysis; multilayered composite and sandwich structures; exact geometry.

1 Introduction

Beams, plates and shells are basic components for the structural analysis in the mechanical, aerospace and civil engineering fields. Numerical models based on these elements allow dynamic, static, free vibration, stability and stress analysis of several structures with different geometries and embedded materials, and subjected to different loading and boundary conditions. Appropriate refined numerical models allow accurate analyses with an increase of safety and a decrease of the weight. However, such numerical models need a deep validation in order to be used with confidence. Such a validation could be made by means of opportune comparisons with exact 3D shell models which have two main advantages: absence of numerical problems in the solution of equations and a complete and exhaustive description

*Corresponding author: Salvatore Brischetto, Department of Mechanical and Aerospace Engineering, Politecnico di Torino, corso Duca degli Abruzzi, 24, 10129 Torino, ITALY. tel: +39.011.090.6813, fax: +39.011.090.6899, e.mail: salvatore.brischetto@polito.it.

of the 3D stress and displacement fields for all the possible thickness ratios and embedded materials of the analyzed structures.

Several 3D exact models have already been presented in the literature. In general, they have been developed for a given geometry and for a restricted choice of materials, lamination sequences and loading conditions. The 3D exact model here proposed tries to overcome these limitations proposing a general shell model valid for spherical shells, cylindrical shells, cylinders and plates. Each investigated structure can be single- or multi-layered (also sandwich and cross-ply configurations) embedding isotropic, orthotropic and composite materials. Loads can be applied at the top/bottom surfaces in terms of transverse shear or transverse normal stresses. For the sake of brevity, the benchmarks here proposed consider transverse normal loads in the z direction applied at the top or at the bottom surfaces. Further loading condition results will be proposed in the near future.

Some of the most important 3D plate models proposed in the literature are described in the following section. Pagano proposed in [1] an elasticity model for the cylindrical bending of composite plates, and in [2] a three-dimensional elasticity model for the static analysis of square and rectangular composite and sandwich plates. Work [1] was extended to uniformly distributed concentrated load cases in [3] by Pagano and Wang. Demasi [4] developed a three-dimensional exact plate solution using the Navier-type method and the mixed form of constitutive equations. The use of the mixed form of Hooke law allows an easier imposition of boundary loading conditions. Aimmanee and Batra [5], [6] proposed the free vibrations of simply-supported plates using analytical solutions. Srinivas et al. [7], [8] developed a 3D linear elastic theory for the free vibration and flexural analysis of simply supported plates subjected to arbitrary loading conditions. Exhaustive comparisons between several 2D theories and an exact 3D plate solution were proposed by Batra et al. [9] for vibration analyses. Ye [10] analyzed the free vibration behaviour of clamped cross-ply plates using a recursive solution. Messina [11] developed an exact three-dimensional plate solution in orthogonal rectilinear coordinates using the exponential matrix method. The same method has been employed in the present new work to write the exact three-dimensional shell solution in general orthogonal curvilinear coordinates. In work [11], Messina investigated free vibrations, displacements and stresses in multilayered plates. The Ritz method applied to develop three-dimensional plate models was used by Cheung and Zhou [12] for isosceles triangular plates and by Liew and Yang [13] for circular plates. The eigenvalue problem, based on the three-dimensional elasticity theory, was solved by Taher et al. [14] and Xing and Liu [15] for free vibration and mode analysis of plates. Exact three-dimensional closed form solutions for free vibrations of Funcionally Graded Material (FGM) plates were proposed by Hosseini-Hashemi et al. [16] for both in-plane and out-of-plane vibration modes. Free and forced vibrations of simply-supported FGM plates were analyzed by Vel and Batra [17] using a three-dimensional exact method. The three-dimensional elastic static analysis of FGM plates, using general expressions for displacements and stresses, was proposed by Xu and Zhou [18]. The free vibration study of a circular piezoelectric plate was performed by Haojiang et al. [19] using a 3D exact model. The cylindrical bending modes for composite simply-supported plates embedding piezoelectric actuators were shown by Baillargeon and Vel [20]. An exact 3D solution was developed for such an analysis. Chen et al. [21] developed a three-dimensional state-space approach to investigate bending and free vibration problems of piezoelectric composite rectangular plates. The same authors developed in [22] an exact 3D model to investigate the distribution of mechanical and electric variables in inner points of a symmetric inhomogeneous multilayered piezoelectric plate. A further study was that by Kapuria and Nair [23] for the exact three-dimensional piezothermoelasticity static, free frequency and steady state harmonic response analysis of composite plates including piezoelectric layers. Zhong and Shang [24] proposed an exact 3D solution for a rectangular plate embedding functionally graded piezoelectric layers using the state space approach. Meyer-Piening [25] proposed results for plate geometries using an elasticity solution valid for sandwich structures. The author declared that such a method could also be extended to curved shell panels.

Elasticity shell solutions are usually less numerous than those for plates because the involved equa-

tions are in general more complicated to be written and to be solved. Among the most important solutions, Ren [26] proposed the exact cylindrical bending elastic analysis of multilayered composite cylindrical shells, and Varadan and Bhaskar [27] developed the three-dimensional elasticity solution of simply supported composite cross-ply cylinders subjected to harmonic loads. Chen et al. [28] used three displacement functions in order to develop a three-dimensional elastic model to analyze the free frequencies of an elastic cylindrical shell. Fan and Zhang [29] wrote the state equations in cylindrical coordinates in order to elaborate a three-dimensional model for static, dynamic and buckling analysis of composite cylindrical panles. The 3D exact theory developed by Gasemzadeh et al. [30] allowed the free frequency analysis of simply-supported cylindrical shells. Huang [31] solved the coupled system of differential equations using the power series method in order to investigate the free frequencies of simply supported composite cylindrical and doubly-curved shells. Sharma et al. [32], [33] used the Fröbenious matrix method to solve the 3D shell equations for the free frequency analysis of homogenous isotropic, viscothermoelastic hollow spheres and trans-radially isotropic, thermoelastic solid spheres. Soldatos and Ye [34] used the exponential matrix to solve the 3D equilibrium equations written in cylindrical coordinates for the free frequency analysis of angle-ply multilayered cylinders. The method proposed in the present new paper also uses the exponential matrix method. However, it is more general than the model by Soldatos and Ye [34] because the use of general orthogonal curvilinear coordinates allows to obtain plate, cylindrical shell and cylinder results as particular cases of the spherical shell analysis. Armenakas et al. [35] introduced a self-contained treatment method based on the three-dimensional theory of elasticity for the free frequency analysis of hollow circular cylinders. Refined 2D models, shear deformation theory, Flügge theory and exact elasticity model are compared in terms of frequencies in [36]. Flügge classical theory for thin shells was detailed in [37] in the case of free frequency analysis of cylindrical shells. Khalili et al. [38] compared two-dimensional closed form models and exact three-dimensional elastic solutions in the case of free frequency analysis of circular cylindrical shells. A first extension of 3D linear elastodynamics equations to FGM cylindrical shells was proposed by Vel [39] using displacement functions to satisfy the boundary conditions. A layer-wise approach, based on the 3D theory of elasticity and on the principle of energy minimization, was proposed by Loy and Lam [40] to study the vibrations of thick circular cylindrical shells. Wang et al. [41] developed the 3D magneto-electro-elastic theory for the free frequency analysis of cylindrical shells. Interesting works by Efraim and Eisenberger [42], Kang and Leissa [43] and Liew et al. [44] were devoted to the 3D free vibration analysis of shells using numerical solutions (e.g., dynamic stiffness matrix method and Ritz method). Fan and Zhang [45] used a methodology similar to that proposed in the present new paper where the 3D equilibrium equations were written in orthogonal curvilinear coordinates for spherical shells. The main difference is between the use of the three displacement components and the three transverse stress components as the six main variables in [45], and the use of the three displacement components and their three derivatives in z as the six main variables in the present work. Moreover, even if the solutions of equations are based on the same principle, they use two different procedures. Fan and Zhang [45] used the Cayley-Hamilton theorem. The procedure employed in the present new paper, based on the exponential matrix method, is able to use of a large number of mathematical layers which allows to analyze in a correct way very thick shells giving a correct 3D behavior for displacements and stresses through the thickness. The use of a large number of mathematical layers could allow an easy extension to FGM structures. Fan and Zhang [45] used the written 3D spherical shell equations to obtain free vibrations and static results for several spherical shell types modifying the curvature from the case of deep spherical shells to shallow spherical shells (plate case is seen as a very shallow spherical shell). The plate results were compared using the equations proposed by Fan and Ye in [46]. The present new work uses the great potentiality of 3D spherical shell equations because they automatically degenerate in those for cylinders and cylindrical panels, when one of the two radii of curvature is imposed as infinite, and in those for plates when both radii of curvature are imposed as infinite. In this way, using the same formulation, static results in terms of displacements and stresses are proposed

for one-layered and multilayered isotropic, orthotropic, sandwich and composite plates, cylinders and cylindrical and spherical shell panels (both thin and thick structures).

Past author's works about exact 3D shell solutions considered only the free vibration analysis of structures. Free frequency analysis of one-layered, multilayered and FGM plates and shells has been conducted in [47], [48] and [49], respectively. Works [50] and [51] analyzed the vibration modes for single-walled carbon nanotubes and double-walled carbon nanotubes, respectively. The convergence analysis of the proposed method, in order to understand the number of mathematical layers and the order of expansion of the exponential matrix, has been proposed in [52]. The shell geometry approximation in the proposed 3D equations for classical and FGM structures has been deeply analyzed in [53] and [54]. Thorough comparisons between the 3D exact shell model and several 2D numerical shell models, in terms of frequency values and vibration modes, have been performed in [55]- [59] for classical and FGM plates and shells and for carbon nanotubes. Free frequency analysis for cylindrical bending vibration modes has been performed in [60] and [61] for classical and FGM structures using both 3D exact and refined 2D numerical models. The present work is the first extension of the 3D exact shell model, used in the past by Brischetto [47]- [61] for free vibration investigations, to static analysis of one-layered and multilayered isotropic, orthotropic, sandwich and composite plates, cylinders and cylindrical/spherical shell panels. The 3D shell equilibrium equations are developed using a general orthogonal curvilinear coordinate system and they are exactly solved via Navier-type conditions and the exponential matrix method. The structures have all the edges as simply supported. Plates and shells are subjected to harmonic transverse normal loads applied at the top or at the bottom surfaces. Results are proposed, giving the three displacement components and the six stress components through the thickness for thin and and thick structures, in order to describe an exhaustive 3D behavior of plates and shells. Proposed benchmarks can be used as reference solutions by those scientists working in the development of plate/shell numerical models which need an appropriate validation.

2 Three-dimensional exact solution for static analysis

In a three-dimensional shell, the middle surface Ω_0 is the locus of points which is situated halfway between the top and the bottom surfaces. The curvilinear orthogonal reference system (α, β, z) is clearly indicated in Figure 1. The distance between the top and bottom surfaces evaluated along the normal to the surface Ω_0 is the thickness h of the structure [62], [63]. The three displacement components are u, v, and w defined along α, β and z directions, respectively.

The parametric quantities for shells having constant radii of curvature (see Figure 1) are:

$$H_\alpha = (1 + \frac{z}{R_\alpha}) = (1 + \frac{\tilde{z} - h/2}{R_\alpha}) \ , \quad H_\beta = (1 + \frac{z}{R_\beta}) = (1 + \frac{\tilde{z} - h/2}{R_\beta}) \ , \quad H_z = 1 \ , \tag{1}$$

H_α and H_β depend on z (which varies from $-h/2$ to $+h/2$ and it is measured starting from Ω_0 surface) or $\tilde{z}$ coordinate (which varies from 0 to h and it is measured starting from bottom surface). R_α and R_β are mean radii of curvature evaluated in α and β directions, respectively [64].

Three-dimensional static study of laminated spherical shells embedding N_L layers, with constant radii of curvature R_α and R_β as indicated in Figure 1, can be implemented using the following differential

equilibrium equations:

$$H_\beta\frac{\partial\sigma^k_{\alpha\alpha}}{\partial\alpha}+H_\alpha\frac{\partial\sigma^k_{\alpha\beta}}{\partial\beta}+H_\alpha H_\beta\frac{\partial\sigma^k_{\alpha z}}{\partial z}+(\frac{2H_\beta}{R_\alpha}+\frac{H_\alpha}{R_\beta})\sigma^k_{\alpha z}=0\ , \tag{2}$$

$$H_\beta\frac{\partial\sigma^k_{\alpha\beta}}{\partial\alpha}+H_\alpha\frac{\partial\sigma^k_{\beta\beta}}{\partial\beta}+H_\alpha H_\beta\frac{\partial\sigma^k_{\beta z}}{\partial z}+(\frac{2H_\alpha}{R_\beta}+\frac{H_\beta}{R_\alpha})\sigma^k_{\beta z}=0\ , \tag{3}$$

$$H_\beta\frac{\partial\sigma^k_{\alpha z}}{\partial\alpha}+H_\alpha\frac{\partial\sigma^k_{\beta z}}{\partial\beta}+H_\alpha H_\beta\frac{\partial\sigma^k_{zz}}{\partial z}-\frac{H_\beta}{R_\alpha}\sigma^k_{\alpha\alpha}-\frac{H_\alpha}{R_\beta}\sigma^k_{\beta\beta}+(\frac{H_\beta}{R_\alpha}+\frac{H_\alpha}{R_\beta})\sigma^k_{zz}=0\ , \tag{4}$$

the most general equations including the case for variable radii of curvature are proposed in [65] and [66]. The six stress components in each k physical layer are $(\sigma^k_{\alpha\alpha},\sigma^k_{\beta\beta},\sigma^k_{zz},\sigma^k_{\beta z},\sigma^k_{\alpha z},\sigma^k_{\alpha\beta})$. R_α and R_β refer to the the mid-surface Ω_0 of the whole laminated shell. H_α and H_β depend on the z coordinate and they continuously vary through the thickness direction of the laminated shell. Symbol ∂ indicates the partial derivatives.

The most general form of three-dimensional strain-displacement relations in the case of general orthogonal curvilinear coordinates were proposed in [64] and [65]. These geometrical relations can be written in a simpler way for shells with constant radii of curvature:

$$\epsilon^k_{\alpha\alpha}=\frac{1}{H_\alpha}\frac{\partial u^k}{\partial\alpha}+\frac{w^k}{H_\alpha R_\alpha}\ , \tag{5}$$

$$\epsilon^k_{\beta\beta}=\frac{1}{H_\beta}\frac{\partial v^k}{\partial\beta}+\frac{w^k}{H_\beta R_\beta}\ , \tag{6}$$

$$\epsilon^k_{zz}=\frac{\partial w^k}{\partial z}\ , \tag{7}$$

$$\gamma^k_{\alpha\beta}=\frac{1}{H_\alpha}\frac{\partial v^k}{\partial\alpha}+\frac{1}{H_\beta}\frac{\partial u^k}{\partial\beta}\ , \tag{8}$$

$$\gamma^k_{\alpha z}=\frac{1}{H_\alpha}\frac{\partial w^k}{\partial\alpha}+\frac{\partial u^k}{\partial z}-\frac{u^k}{H_\alpha R_\alpha}\ , \tag{9}$$

$$\gamma^k_{\beta z}=\frac{1}{H_\beta}\frac{\partial w^k}{\partial\beta}+\frac{\partial v^k}{\partial z}-\frac{v^k}{H_\beta R_\beta}\ . \tag{10}$$

Eqs.(5)-(10) are written for spherical shells and they degenerate into equations for cylindrical shells when R_α or R_β is infinite (which means H_α or H_β equals one), and they degenerate into equations for plates when both R_α and R_β are infinite (which means H_α=H_β=1). $(\epsilon^k_{\alpha\alpha},\epsilon^k_{\beta\beta},\epsilon^k_{zz},\gamma^k_{\beta z},\gamma^k_{\alpha z},\gamma^k_{\alpha\beta})$ are the six strain components for each k physical layer.

3D linear elastic constitutive relations link the stress components with the strain components by means of elastic coefficients C^k_{ij}. For a generic orthotropic material in the structural reference system (α, β, z) and considering a generic k layer of the multilayered plate or shell, these equations are:

$$\sigma^k_{\alpha\alpha}=C^k_{11}\epsilon^k_{\alpha\alpha}+C^k_{12}\epsilon^k_{\beta\beta}+C^k_{13}\epsilon^k_{zz}+C^k_{16}\gamma^k_{\alpha\beta}\ , \tag{11}$$

$$\sigma^k_{\beta\beta}=C^k_{12}\epsilon^k_{\alpha\alpha}+C^k_{22}\epsilon^k_{\beta\beta}+C^k_{23}\epsilon^k_{zz}+C^k_{26}\gamma^k_{\alpha\beta}\ , \tag{12}$$

$$\sigma^k_{zz}=C^k_{13}\epsilon^k_{\alpha\alpha}+C^k_{23}\epsilon^k_{\beta\beta}+C^k_{33}\epsilon^k_{zz}+C^k_{36}\gamma^k_{\alpha\beta}\ , \tag{13}$$

$$\sigma^k_{\beta z}=C^k_{44}\gamma^k_{\beta z}+C^k_{45}\gamma^k_{\alpha z}\ , \tag{14}$$

$$\sigma^k_{\alpha z}=C^k_{45}\gamma^k_{\beta z}+C^k_{55}\gamma^k_{\alpha z}\ , \tag{15}$$

$$\sigma^k_{\alpha\beta}=C^k_{16}\epsilon^k_{\alpha\alpha}+C^k_{26}\epsilon^k_{\beta\beta}+C^k_{36}\epsilon^k_{zz}+C^k_{66}\gamma^k_{\alpha\beta}\ . \tag{16}$$

Closed form solution of Eqs.(2)-(4) is possible only if cross-ply laminates are considered (which means fibre orientation angle θ equals 0° or 90°). This last feature means elastic coefficients C^k_{16}, C^k_{26}, C^k_{36} and

C^k_{45} equal zero. This condition combined with the substitution of Eqs.(5)-(10) into Eqs.(11)-(16) leads to the employed constitutive equations:

$$\sigma^k_{\alpha\alpha} = \frac{C^k_{11}}{H_\alpha}u^k_{,\alpha} + \frac{C^k_{11}}{H_\alpha R_\alpha}w^k + \frac{C^k_{12}}{H_\beta}v^k_{,\beta} + \frac{C^k_{12}}{H_\beta R_\beta}w^k + C^k_{13}w^k_{,z} \ , \tag{17}$$

$$\sigma^k_{\beta\beta} = \frac{C^k_{12}}{H_\alpha}u^k_{,\alpha} + \frac{C^k_{12}}{H_\alpha R_\alpha}w^k + \frac{C^k_{22}}{H_\beta}v^k_{,\beta} + \frac{C^k_{22}}{H_\beta R_\beta}w^k + C^k_{23}w^k_{,z} \ , \tag{18}$$

$$\sigma^k_{zz} = \frac{C^k_{13}}{H_\alpha}u^k_{,\alpha} + \frac{C^k_{13}}{H_\alpha R_\alpha}w^k + \frac{C^k_{23}}{H_\beta}v^k_{,\beta} + \frac{C^k_{23}}{H_\beta R_\beta}w^k + C^k_{33}w^k_{,z} \ , \tag{19}$$

$$\sigma^k_{\beta z} = \frac{C^k_{44}}{H_\beta}w^k_{,\beta} + C^k_{44}v^k_{,z} - \frac{C^k_{44}}{H_\beta R_\beta}v^k \ , \tag{20}$$

$$\sigma^k_{\alpha z} = \frac{C^k_{55}}{H_\alpha}w^k_{,\alpha} + C^k_{55}u^k_{,z} - \frac{C^k_{55}}{H_\alpha R_\alpha}u^k \ , \tag{21}$$

$$\sigma^k_{\alpha\beta} = \frac{C^k_{66}}{H_\alpha}v^k_{,\alpha} + \frac{C^k_{66}}{H_\beta}u^k_{,\beta} \ . \tag{22}$$

Symbol for partial derivatives $\frac{\partial}{\partial\alpha}$, $\frac{\partial}{\partial\beta}$ and $\frac{\partial}{\partial z}$ are here replaced by subscripts $_{,\alpha}$, $_{,\beta}$ and $_{,z}$, respectively.

Equilibrium equations (2)-(4) for a generic physical layer k can be written in displacement form via substitution of constitutive equations (17)-(22):

$$\begin{aligned}
&\Big(-\frac{H_\beta C^k_{55}}{H_\alpha R^2_\alpha} - \frac{C^k_{55}}{R_\alpha R_\beta}\Big)u^k + \Big(\frac{C^k_{55}H_\beta}{R_\alpha} + \frac{C^k_{55}H_\alpha}{R_\beta}\Big)u^k_{,z} + \Big(\frac{C^k_{11}H_\beta}{H_\alpha}\Big)u^k_{,\alpha\alpha} + \Big(\frac{C^k_{66}H_\alpha}{H_\beta}\Big)u^k_{,\beta\beta} + \\
&\Big(C^k_{55}H_\alpha H_\beta\Big)u^k_{,zz} + \Big(C^k_{12} + C^k_{66}\Big)v^k_{,\alpha\beta} + \Big(\frac{C^k_{11}H_\beta}{H_\alpha R_\alpha} + \frac{C^k_{12}}{R_\beta} + \frac{C^k_{55}H_\beta}{H_\alpha R_\alpha} + \frac{C^k_{55}}{R_\beta}\Big)w^k_{,\alpha} + \\
&\Big(C^k_{13}H_\beta + C^k_{55}H_\beta\Big)w^k_{,\alpha z} = 0 \ ,
\end{aligned} \tag{23}$$

$$\begin{aligned}
&\Big(-\frac{H_\alpha C^k_{44}}{H_\beta R^2_\beta} - \frac{C^k_{44}}{R_\alpha R_\beta}\Big)v^k + \Big(\frac{C^k_{44}H_\alpha}{R_\beta} + \frac{C^k_{44}H_\beta}{R_\alpha}\Big)v^k_{,z} + \Big(\frac{C^k_{66}H_\beta}{H_\alpha}\Big)v^k_{,\alpha\alpha} + \Big(\frac{C^k_{22}H_\alpha}{H_\beta}\Big)v^k_{,\beta\beta} + \\
&\Big(C^k_{44}H_\alpha H_\beta\Big)v^k_{,zz} + \Big(C^k_{12} + C^k_{66}\Big)u^k_{,\alpha\beta} + \Big(\frac{C^k_{44}H_\alpha}{H_\beta R_\beta} + \frac{C^k_{44}}{R_\alpha} + \frac{C^k_{22}H_\alpha}{H_\beta R_\beta} + \frac{C^k_{12}}{R_\alpha}\Big)w^k_{,\beta} + \\
&\Big(C^k_{44}H_\alpha + C^k_{23}H_\alpha\Big)w^k_{,\beta z} = 0 \ ,
\end{aligned} \tag{24}$$

$$\begin{aligned}
&\Big(\frac{C^k_{13}}{R_\alpha R_\beta} + \frac{C^k_{23}}{R_\alpha R_\beta} - \frac{C^k_{11}H_\beta}{H_\alpha R^2_\alpha} - \frac{2C^k_{12}}{R_\alpha R_\beta} - \frac{C^k_{22}H_\alpha}{H_\beta R^2_\beta}\Big)w^k + \Big(-\frac{C^k_{55}H_\beta}{H_\alpha R_\alpha} + \frac{C^k_{13}}{R_\beta} - \frac{C^k_{11}H_\beta}{H_\alpha R_\alpha} - \frac{C^k_{12}}{R_\beta}\Big)u^k_{,\alpha} + \\
&\Big(-\frac{C^k_{44}H_\alpha}{H_\beta R_\beta} + \frac{C^k_{23}}{R_\alpha} - \frac{C^k_{22}H_\alpha}{H_\beta R_\beta} - \frac{C^k_{12}}{R_\alpha}\Big)v^k_{,\beta} + \Big(\frac{C^k_{33}H_\beta}{R_\alpha} + \frac{C^k_{33}H_\alpha}{R_\beta}\Big)w^k_{,z} + \\
&\Big(C^k_{55}H_\beta + C^k_{13}H_\beta\Big)u^k_{,\alpha z} + \Big(C^k_{44}H_\alpha + C^k_{23}H_\alpha\Big)v^k_{,\beta z} + \Big(C^k_{55}\frac{H_\beta}{H_\alpha}\Big)w^k_{,\alpha\alpha} + \Big(C^k_{44}\frac{H_\alpha}{H_\beta}\Big)w^k_{,\beta\beta} + \\
&\Big(C^k_{33}H_\alpha H_\beta\Big)w^k_{,zz} = 0 \ .
\end{aligned} \tag{25}$$

Eqs.(23)-(25) are written in closed form supposing simply supported egdes in all the considered structures and using harmonic forms for the three displacement components:

$$u^k(\alpha,\beta,z) = U^k(z)cos(\bar\alpha\alpha)sin(\bar\beta\beta) \ , \tag{26}$$

$$v^k(\alpha,\beta,z) = V^k(z)sin(\bar\alpha\alpha)cos(\bar\beta\beta) \ , \tag{27}$$

$$w^k(\alpha,\beta,z) = W^k(z)sin(\bar\alpha\alpha)sin(\bar\beta\beta) \ , \tag{28}$$

where U^k, V^k and W^k are the amplitudes for displacements evaluated in α, β and z directions, respectively. Coefficients $\bar{\alpha} = \frac{m\pi}{a}$ and $\bar{\beta} = \frac{n\pi}{b}$ include m and n as the half-wave numbers and a and b as the shell dimensions in α and β directions, respectively (all these quantities are calculated at the mid-surface Ω_0). R_α and R_β are measured at the reference mid-surface Ω_0 of the multilayered shell. H_α and H_β are evaluated through the thickness direction of the laminated shell using Eq.(1). Equilibrium relations are written for spherical shells, they automatically degenerate into equilibrium relations for cylindrical closed/open shells when R_α or R_β is infinite (which means H_α or H_β equals one) and into equilibrium relations for plates [11] when R_α and R_β are infinite (which means H_α and H_β equal one). These features allow a unified and general formulation valid for all the considered geometries.

Eqs.(26)-(28) are substituted in Eqs.(23)-(25) in order to obtain the equilibrium equations in terms of displacement amplitudes and their derivatives made with respect to z coordinate:

$$\begin{aligned}
&\Big(- \frac{C^k_{55}H_\beta}{H_\alpha R^2_\alpha} - \frac{C^k_{55}}{R_\alpha R_\beta} - \bar{\alpha}^2\frac{C^k_{11}H_\beta}{H_\alpha} - \bar{\beta}^2\frac{C^k_{66}H_\alpha}{H_\beta}\Big)U^k + \Big(- \bar{\alpha}\bar{\beta}C^k_{12} - \bar{\alpha}\bar{\beta}C^k_{66}\Big)V^k + \\
&\Big(\bar{\alpha}\frac{C^k_{11}H_\beta}{H_\alpha R_\alpha} + \bar{\alpha}\frac{C^k_{12}}{R_\beta} + \bar{\alpha}\frac{C^k_{55}H_\beta}{H_\alpha R_\alpha} + \bar{\alpha}\frac{C^k_{55}}{R_\beta}\Big)W^k + \Big(\frac{C^k_{55}H_\beta}{R_\alpha} + \frac{C^k_{55}H_\alpha}{R_\beta}\Big)U^k_{,z} + \Big(\bar{\alpha}C^k_{13}H_\beta + \\
&\bar{\alpha}C^k_{55}H_\beta\Big)W^k_{,z} + \Big(C^k_{55}H_\alpha H_\beta\Big)U^k_{,zz} = 0\,,
\end{aligned} \tag{29}$$

$$\begin{aligned}
&\Big(- \bar{\alpha}\bar{\beta}C^k_{66} - \bar{\alpha}\bar{\beta}C^k_{12}\Big)U^k + \Big(- \frac{C^k_{44}H_\alpha}{H_\beta R^2_\beta} - \frac{C^k_{44}}{R_\alpha R_\beta} - \bar{\alpha}^2\frac{C^k_{66}H_\beta}{H_\alpha} - \bar{\beta}^2\frac{C^k_{22}H_\alpha}{H_\beta}\Big)V^k + \\
&\Big(\bar{\beta}\frac{C^k_{44}H_\alpha}{H_\beta R_\beta} + \bar{\beta}\frac{C^k_{44}}{R_\alpha} + \bar{\beta}\frac{C^k_{22}H_\alpha}{H_\beta R_\beta} + \bar{\beta}\frac{C^k_{12}}{R_\alpha}\Big)W^k + \Big(\frac{C^k_{44}H_\alpha}{R_\beta} + \frac{C^k_{44}H_\beta}{R_\alpha}\Big)V^k_{,z} + \Big(\bar{\beta}C^k_{44}H_\alpha + \\
&\bar{\beta}C^k_{23}H_\alpha\Big)W^k_{,z} + \Big(C^k_{44}H_\alpha H_\beta\Big)V^k_{,zz} = 0\,,
\end{aligned} \tag{30}$$

$$\begin{aligned}
&\Big(\bar{\alpha}\frac{C^k_{55}H_\beta}{H_\alpha R_\alpha} - \bar{\alpha}\frac{C^k_{13}}{R_\beta} + \bar{\alpha}\frac{C^k_{11}H_\beta}{H_\alpha R_\alpha} + \bar{\alpha}\frac{C^k_{12}}{R_\beta}\Big)U^k + \Big(\bar{\beta}\frac{C^k_{44}H_\alpha}{H_\beta R_\beta} - \bar{\beta}\frac{C^k_{23}}{R_\alpha} + \bar{\beta}\frac{C^k_{22}H_\alpha}{H_\beta R_\beta} + \bar{\beta}\frac{C^k_{12}}{R_\alpha}\Big)V^k + \\
&\Big(\frac{C^k_{13}}{R_\alpha R_\beta} + \frac{C^k_{23}}{R_\alpha R_\beta} - \frac{C^k_{11}H_\beta}{H_\alpha R^2_\alpha} - \frac{2C^k_{12}}{R_\alpha R_\beta} - \frac{C^k_{22}H_\alpha}{H_\beta R^2_\beta} - \bar{\alpha}^2\frac{C^k_{55}H_\beta}{H_\alpha} - \bar{\beta}^2\frac{C^k_{44}H_\alpha}{H_\beta}\Big)W^k + \\
&\Big(- \bar{\alpha}C^k_{55}H_\beta - \bar{\alpha}C^k_{13}H_\beta\Big)U^k_{,z} + \Big(- \bar{\beta}C^k_{44}H_\alpha - \bar{\beta}C^k_{23}H_\alpha\Big)V^k_{,z} + \Big(\frac{C^k_{33}H_\beta}{R_\alpha} + \frac{C^k_{33}H_\alpha}{R_\beta}\Big)W^k_{,z} + \\
&\Big(C^k_{33}H_\alpha H_\beta\Big)W^k_{,zz} = 0\,.
\end{aligned} \tag{31}$$

Eqs.(29)-(31) are a system of three second order partial differential relations in z. These equations are proposed for spherical shells with constant radii of curvature and they can easily degenerate into relations for cylindrical panels and plates. A compact form can be proposed when coefficients A^k_s are used in place of each block $\Big(\Big)$ with k indicating the physical layer and index s varying from 1 to 19:

$$A^k_1U^k + A^k_2V^k + A^k_3W^k + A^k_4U^k_{,z} + A^k_5W^k_{,z} + A^k_6U^k_{,zz} = 0\,, \tag{32}$$

$$A^k_7U^k + A^k_8V^k + A^k_9W^k + A^k_{10}V^k_{,z} + A^k_{11}W^k_{,z} + A^k_{12}V^k_{,zz} = 0\,, \tag{33}$$

$$A^k_{13}U^k + A^k_{14}V^k + A^k_{15}W^k + A^k_{16}U^k_{,z} + A^k_{17}V^k_{,z} + A^k_{18}W^k_{,z} + A^k_{19}W^k_{,zz} = 0\,. \tag{34}$$

The method described in [67] and [68] allows the reduction of the system of second order differential equations in a system of first order differential equations simply using the redouble of the variables (all

the details, here omitted for the sake of brevity, are given in [48]). The new system is:

$$\begin{bmatrix} A_6^k & 0 & 0 & 0 & 0 & 0 \\ 0 & A_{12}^k & 0 & 0 & 0 & 0 \\ 0 & 0 & A_{19}^k & 0 & 0 & 0 \\ 0 & 0 & 0 & A_6^k & 0 & 0 \\ 0 & 0 & 0 & 0 & A_{12}^k & 0 \\ 0 & 0 & 0 & 0 & 0 & A_{19}^k \end{bmatrix} \begin{bmatrix} U^k \\ V^k \\ W^k \\ U^{k\prime} \\ V^{k\prime} \\ W^{k\prime} \end{bmatrix}' = \begin{bmatrix} 0 & 0 & 0 & A_6^k & 0 & 0 \\ 0 & 0 & 0 & 0 & A_{12}^k & 0 \\ 0 & 0 & 0 & 0 & 0 & A_{19}^k \\ -A_1^k & -A_2^k & -A_3^k & -A_4^k & 0 & -A_5^k \\ -A_7^k & -A_8^k & -A_9^k & 0 & -A_{10}^k & -A_{11}^k \\ -A_{13}^k & -A_{14}^k & -A_{15}^k & -A_{16}^k & -A_{17}^k & -A_{18}^k \end{bmatrix} \begin{bmatrix} U^k \\ V^k \\ W^k \\ U^{k\prime} \\ V^{k\prime} \\ W^{k\prime} \end{bmatrix} . \tag{35}$$

Considering a generic k layer, Eq.(35) can be proposed as:

$$\boldsymbol{D}^k \frac{\partial \boldsymbol{U}^k}{\partial \tilde{z}} = \boldsymbol{A}^k \boldsymbol{U}^k \ , \tag{36}$$

where $\frac{\partial \boldsymbol{U}^k}{\partial \tilde{z}} = \boldsymbol{U}^{k\prime}$ and $\boldsymbol{U}^k = [U^k \ V^k \ W^k \ U^{k\prime} \ V^{k\prime} \ W^{k\prime}]$. Further steps must be performed:

$$\boldsymbol{D}^k \boldsymbol{U}^{k\prime} = \boldsymbol{A}^k \boldsymbol{U}^k \ , \tag{37}$$

$$\boldsymbol{U}^{k\prime} = \boldsymbol{D}^{k^{-1}} \boldsymbol{A}^k \ \boldsymbol{U}^k \ , \tag{38}$$

$$\boldsymbol{U}^{k\prime} = \boldsymbol{A}^{k*} \ \boldsymbol{U}^k \ , \tag{39}$$

with $\boldsymbol{A}^{k*} = \boldsymbol{D}^{k^{-1}} \boldsymbol{A}^k$. Plates have coefficients A_3^k, A_4^k, A_9^k, A_{10}^k, A_{13}^k, A_{14}^k and A_{18}^k equal zero because of infinite radii of curvature R_α and R_β. The remaining coefficients A_1^k, A_2^k, A_5^k, A_6^k, A_7^k, A_8^k, A_{11}^k, A_{12}^k, A_{15}^k, A_{16}^k, A_{17}^k and A_{19}^k are constant in each k layer because parametric coefficients $H_\alpha = H_\beta = 1$ do not depend on the thickness coordinate $\tilde{z}$ in the case of plates. Therefore, matrices $\boldsymbol{D}^k$, $\boldsymbol{A}^k$ and $\boldsymbol{A}^{k*}$ are constant in each k layer of the plate. The solution of Eq.(39) for plates can be written as proposed in [68] and [69]:

$$\boldsymbol{U}^k(\tilde{z}^k) = exp(\boldsymbol{A}^{k*} \tilde{z}^k) \boldsymbol{U}^k(0) \quad \text{with} \quad \tilde{z}^k \ \epsilon \ [0, h^k] \ , \tag{40}$$

where $\tilde{z}^k$ is the coordinate through the thickness of each layer k from 0 at the bottom to h^k at the top. The exponential matrix for the plate geometry (constant coefficients A_s^k) is developed with $\tilde{z}^k = h^k$ for each k layer:

$$\boldsymbol{A}^{k**} = exp(\boldsymbol{A}^{k*} h^k) = \boldsymbol{I} + \boldsymbol{A}^{k*} \ h^k + \frac{\boldsymbol{A}^{k*2}}{2!} h^{k2} + \frac{\boldsymbol{A}^{k*3}}{3!} h^{k3} + \ldots + \frac{\boldsymbol{A}^{k*N}}{N!} h^{kN} \ , \tag{41}$$

where $\boldsymbol{I}$ is the 6×6 identity matrix. This expansion has a very rapid convergence as demonstrated in [70]. For this reason, the method is not time consuming from the computational point of view. Brischetto [49] demonstrated as $N = 15$ order of expansion gives the exact solution for free vibration analysis of each possible one-layered plate case. For one-layered and multilayered shells embedding one or N_L physical layers, $\boldsymbol{A}^{k*}$ is not constant in each k layer because parametric coefficients $H_\alpha(\tilde{z})$ and $H_\beta(\tilde{z})$ depend on the thickness coordinate. Matrices $\boldsymbol{D}^k$, $\boldsymbol{A}^k$ and $\boldsymbol{A}^{k*}$ are constant in each k layer when radii of curvature R_α and R_β are infinite for the multilayered plate cases (this condition means $H_\alpha = H_\beta = 1$). Shell structures have not constant matrices $\boldsymbol{D}^k$, $\boldsymbol{A}^k$ and $\boldsymbol{A}^{k*}$ because parametric coefficients H_α and H_β in each k layer depend on the thickness coordinate $\tilde{z}$. In shell cases, the introduction of several q fictitious/mathematical layers in each k layer is mandatory in order to exactly evaluate H_α and H_β. In this work, each k physical layer of the laminated shell will be divided in an opportune number of q mathematical layers in order to obtain a total number M of layers with index j and constant thickness h_j. In this way, all the above-quoted equations must be rewritten with index j in place of index k in order to be valid for shell structures. Index j considers the total physical and mathematical layers obtained dividing the k physical layers in mathematical layers with constant thickness. In this way, matrices $\boldsymbol{A}^{j**}$ are constant in each mathematical j layer because they can be

calculated using R_α, R_β, $\bar{\alpha}$ and $\bar{\beta}$ evaluated at the mid-surface Ω_0 of the whole shell, and using H_α and H_β evaluated in the middle of each j layer.

In the case of multilayered shells, $M-1$ transfer matrices $\boldsymbol{T}^{j-1,j}$ must be defined. These matrices are obtained writing for each interface (physical or mathematical interface) the conditions to impose the interlaminar continuity of displacements and transverse shear/normal stresses:

$$u_b^j = u_t^{j-1}\,,\;\; v_b^j = v_t^{j-1}\,,\;\; w_b^j = w_t^{j-1}\,, \tag{42}$$

$$\sigma_{zzb}^j = \sigma_{zzt}^{j-1}\,,\;\; \sigma_{\alpha zb}^j = \sigma_{\alpha zt}^{j-1}\,,\;\; \sigma_{\beta zb}^j = \sigma_{\beta zt}^{j-1}\,, \tag{43}$$

each displacement and transverse stress component at the top (t) of the j-1 layer is equal to the connected displacement and transverse stress component at the bottom (b) of the j layer.

The continuity of transverse shear stress $\sigma_{\alpha z}$ as suggested in Eq.(43) can be written in explicit form using Eq.(21) and index j:

$$\frac{C_{55}^{j-1}}{H_{\alpha t}^{j-1}}\bar{\alpha}W_t^{j-1} + C_{55}^{j-1}U_t^{j-1\prime} - \frac{C_{55}^{j-1}}{H_{\alpha t}^{j-1}R_\alpha}U_t^{j-1} = \frac{C_{55}^{j}}{H_{\alpha b}^{j}}\bar{\alpha}W_b^{j} + C_{55}^{j}U_b^{j\prime} - \frac{C_{55}^{j}}{H_{\alpha b}^{j}R_\alpha}U_b^{j}\,, \tag{44}$$

$$U_b^{j\prime} = \frac{1}{C_{55}^j}\Big(\frac{C_{55}^{j-1}}{H_{\alpha t}^{j-1}}\bar{\alpha} - \frac{C_{55}^{j}}{H_{\alpha b}^{j}}\bar{\alpha}\Big)W_t^{j-1} + \frac{1}{C_{55}^j}\Big(-\frac{C_{55}^{j-1}}{H_{\alpha t}^{j-1}R_\alpha} + \frac{C_{55}^{j}}{H_{\alpha b}^{j}R_\alpha}\Big)U_t^{j-1} + \Big(\frac{C_{55}^{j-1}}{C_{55}^{j}}\Big)U_t^{j-1\prime}\,. \tag{45}$$

The continuity of transverse shear stress $\sigma_{\beta z}$ as suggested in Eq.(43) can be written in explicit form using Eq.(20) and index j:

$$\frac{C_{44}^{j-1}}{H_{\beta t}^{j-1}}\bar{\beta}W_t^{j-1} + C_{44}^{j-1}V_t^{j-1\prime} - \frac{C_{44}^{j-1}}{H_{\beta t}^{j-1}R_\beta}V_t^{j-1} = \frac{C_{44}^{j}}{H_{\beta b}^{j}}\bar{\beta}W_b^{j} + C_{44}^{j}V_b^{j\prime} - \frac{C_{44}^{j}}{H_{\beta b}^{j}R_\beta}V_b^{j}\,, \tag{46}$$

$$V_b^{j\prime} = \frac{1}{C_{44}^j}\Big(\frac{C_{44}^{j-1}}{H_{\beta t}^{j-1}}\bar{\beta} - \frac{C_{44}^{j}}{H_{\beta b}^{j}}\bar{\beta}\Big)W_t^{j-1} + \frac{1}{C_{44}^j}\Big(-\frac{C_{44}^{j-1}}{H_{\beta t}^{j-1}R_\beta} + \frac{C_{44}^{j}}{H_{\beta b}^{j}R_\beta}\Big)V_t^{j-1} + \Big(\frac{C_{44}^{j-1}}{C_{44}^{j}}\Big)V_t^{j-1\prime}\,. \tag{47}$$

The continuity of transverse shear stress σ_{zz} as suggested in Eq.(43) can be written in explicit form using Eq.(19) and index j:

$$\begin{aligned} &-\frac{C_{13}^{j-1}}{H_{\alpha t}^{j-1}}\bar{\alpha}U_t^{j-1} + \frac{C_{13}^{j-1}}{H_{\alpha t}^{j-1}R_\alpha}W_t^{j-1} - \frac{C_{23}^{j-1}}{H_{\beta t}^{j-1}}\bar{\beta}V_t^{j-1} + \frac{C_{23}^{j-1}}{H_{\beta t}^{j-1}R_\beta}W_t^{j-1} + C_{33}^{j-1}W_t^{j-1\prime} = \\ &-\frac{C_{13}^{j}}{H_{\alpha b}^{j}}\bar{\alpha}U_b^{j} + \frac{C_{13}^{j}}{H_{\alpha b}^{j}R_\alpha}W_b^{j} - \frac{C_{23}^{j}}{H_{\beta b}^{j}}\bar{\beta}V_b^{j} + \frac{C_{23}^{j}}{H_{\beta b}^{j}R_\beta}W_b^{j} + C_{33}^{j}W_b^{j\prime}\,, \end{aligned} \tag{48}$$

$$\begin{aligned} W_b^{j\prime} = {}& \frac{1}{C_{33}^j}\Big(-\frac{C_{13}^{j-1}}{H_{\alpha t}^{j-1}}\bar{\alpha} + \frac{C_{13}^{j}}{H_{\alpha b}^{j}}\bar{\alpha}\Big)U_t^{j-1} + \frac{1}{C_{33}^j}\Big(-\frac{C_{23}^{j-1}}{H_{\beta t}^{j-1}}\bar{\beta} + \frac{C_{23}^{j}}{H_{\beta b}^{j}}\bar{\beta}\Big)V_t^{j-1} + \\ & \frac{1}{C_{33}^j}\Big(\frac{C_{13}^{j-1}}{H_{\alpha t}^{j-1}R_\alpha} + \frac{C_{23}^{j-1}}{H_{\beta t}^{j-1}R_\beta} - \frac{C_{13}^{j}}{H_{\alpha b}^{j}R_\alpha} - \frac{C_{23}^{j}}{H_{\beta b}^{j}R_\beta}\Big)W_t^{j-1} + \Big(\frac{C_{33}^{j-1}}{C_{33}^{j}}\Big)W_t^{j-1\prime}\,. \end{aligned} \tag{49}$$

The continuity of displacement components (see Eq.(42)), written in terms of amplitude and using the harmonic forms as already done in Eqs.(44)-(49), is:

$$U_b^j = U_t^{j-1}\,,\;\; V_b^j = V_t^{j-1}\,,\;\; W_b^j = W_t^{j-1}\,. \tag{50}$$

In above-mentioned equations, t and b indicate top and bottom of $j-1$ layer and j layer, respectively. $\bar{\alpha}$, $\bar{\beta}$, R_α and R_β are measured with respect to the mid-surface Ω_0 of the structure. H_α and H_β are evaluated where it has been indicated by the subscript b or t and the superscript j or $j-1$.

The conditions summarized in Eqs.(45), (47), (49) and (50) can be rewritten using the following system:

$$\begin{bmatrix} U \\ V \\ W \\ U' \\ V' \\ W' \end{bmatrix}_b^j = \begin{bmatrix} 1 & 0 & 0 & 0 & 0 & 0 \\ 0 & 1 & 0 & 0 & 0 & 0 \\ 0 & 0 & 1 & 0 & 0 & 0 \\ T_1 & 0 & T_2 & T_3 & 0 & 0 \\ 0 & T_4 & T_5 & 0 & T_6 & 0 \\ T_7 & T_8 & T_9 & 0 & 0 & T_{10} \end{bmatrix}^{j-1,j} \begin{bmatrix} U \\ V \\ W \\ U' \\ V' \\ W' \end{bmatrix}_t^{j-1} , \tag{51}$$

The compact form of Eq.(51) is:

$$\boldsymbol{U}_b^j = \boldsymbol{T}^{j-1,j} \boldsymbol{U}_t^{j-1} . \tag{52}$$

The matrices $\boldsymbol{T}^{j-1,j}$ links $\boldsymbol{U}$ defined at the bottom (b) of the j layer with $\boldsymbol{U}$ defined at the top (t) of the $j-1$ layer. This condition can also be expressed as:

$$\boldsymbol{U}^j(0) = \boldsymbol{T}^{j-1,j} \; \boldsymbol{U}^{j-1}(h^{j-1}) , \tag{53}$$

displacements $\boldsymbol{U}^j$ are evaluated at $\tilde{z}^j = 0$ and displacements $\boldsymbol{U}^{j-1}$ are evaluated at $\tilde{z}^{j-1} = h^{j-1}$. $\boldsymbol{U}$ at the top of the j layer and $\boldsymbol{U}$ at the bottom of the same j layer are linked via the exponential matrix $\boldsymbol{A}^{j**}$ as suggested in Eqs.(40) and (41):

$$\boldsymbol{U}^j(h^j) = \boldsymbol{A}^{j**} \; \boldsymbol{U}^j(0) , \tag{54}$$

Eq.(53) can recursively be included in Eq.(54) for each $M-1$ interface:

$$\boldsymbol{U}^M(h^M) = \boldsymbol{A}^{M**} \; \boldsymbol{T}^{M-1,M} \; \boldsymbol{A}^{M-1**} \; \boldsymbol{T}^{M-2,M-1} \ldots\ldots \boldsymbol{A}^{2**} \; \boldsymbol{T}^{1,2} \; \boldsymbol{A}^{1**} \; \boldsymbol{U}^1(0) , \tag{55}$$

defining the matrix $\boldsymbol{H}_m$ in the case of multilayered structures, Eq.(55) can be rewritten as:

$$\boldsymbol{U}^M(h^M) = \boldsymbol{H}_m \; \boldsymbol{U}^1(0) , \tag{56}$$

Eq.(56) links $\boldsymbol{U}$ defined at the top of the last M layer with $\boldsymbol{U}$ evaluated at the bottom of the first layer. Matrices $\boldsymbol{T}^{j-1,j}$ become constant because they are calculated using R_α, R_β, $\bar{\alpha}$ and $\bar{\beta}$ evaluated at the mid-surface Ω_0 of the shell, and using H_α and H_β evaluated at each mathematical/fictitious interface.

The analyzed plates and shells have simply supported edges and they can be loaded at the top and/or at the bottom of the whole laminated structure using the following conditions:

$$\sigma_{zz} = p_z , \quad \sigma_{\alpha z} = p_\alpha , \quad \sigma_{\beta z} = p_\beta \quad \text{for} \quad z = -h/2, +h/2 \quad or \quad \tilde{z} = 0, h , \tag{57}$$

$$w = v = 0, \; \sigma_{\alpha\alpha} = 0 \quad \text{for} \quad \alpha = 0, a , \tag{58}$$

$$w = u = 0, \; \sigma_{\beta\beta} = 0 \quad \text{for} \quad \beta = 0, b , \tag{59}$$

p_z, p_α and p_β are harmonic mechanical loads that can be applied at the top or at the bottom of the structure in z, α and β direction, respectively:

$$p_\alpha^j(\alpha, \beta, z) = P_\alpha^j(z) cos(\bar{\alpha}\alpha) sin(\bar{\beta}\beta) , \tag{60}$$

$$p_\beta^j(\alpha, \beta, z) = P_\beta^j(z) sin(\bar{\alpha}\alpha) cos(\bar{\beta}\beta) , \tag{61}$$

$$p_z^j(\alpha, \beta, z) = P_z^j(z) sin(\bar{\alpha}\alpha) sin(\bar{\beta}\beta) , \tag{62}$$

P_α^j, P_β^j and P_z^j indicate the load amplitudes.

Transverse shear/normal stresses developed for a generic value of $\tilde{z}$ in the j layer are:

$$\sigma^j_{zz}(\tilde{z}) = \frac{C^j_{13}}{H_\alpha(\tilde{z})}u^j_{,\alpha} + \frac{C^j_{13}}{H_\alpha(\tilde{z})R_\alpha}w^j + \frac{C^j_{23}}{H_\beta(\tilde{z})}v^j_{,\beta} + \frac{C^j_{23}}{H_\beta(\tilde{z})R_\beta}w^j + C^j_{33}w^j_{,z} = -\bar{\alpha}\frac{C^j_{13}}{H_\alpha(\tilde{z})}U^j + \frac{C^j_{13}}{H_\alpha(\tilde{z})R_\alpha}W^j - \bar{\beta}\frac{C^j_{23}}{H_\beta(\tilde{z})}V^j + \frac{C^j_{23}}{H_\beta(\tilde{z})R_\beta}W^j + C^j_{33}W^j_{,z}\,, \tag{63}$$

$$\sigma^j_{\beta z}(\tilde{z}) = \frac{C^j_{44}}{H_\beta(\tilde{z})}w^j_{,\beta} + C^j_{44}v^j_{,z} - \frac{C^j_{44}}{H_\beta(\tilde{z})R_\beta}v^j = \bar{\beta}\frac{C^j_{44}}{H_\beta(\tilde{z})}W^j + C^j_{44}V^j_{,z} - \frac{C^j_{44}}{H_\beta(\tilde{z})R_\beta}V^j\,, \tag{64}$$

$$\sigma^j_{\alpha z}(\tilde{z}) = \frac{C^j_{55}}{H_\alpha(\tilde{z})}w^j_{,\alpha} + C^j_{55}u^j_{,z} - \frac{C^j_{55}}{H_\alpha(\tilde{z})R_\alpha}u^j = \bar{\alpha}\frac{C^j_{55}}{H_\alpha(\tilde{z})}W^j + C^j_{55}U^j_{,z} - \frac{C^j_{55}}{H_\alpha(\tilde{z})R_\alpha}U^j\,, \tag{65}$$

Eqs.(63)-(65) written at the the top (t) of the last j layer use the conditions summarized by Eq.(57) with R_α, R_β, $\bar{\alpha}$ and $\bar{\beta}$ evaluated at the mid-surface Ω_0 of the shell, and with H^t_α and H^t_β defined at top of the whole structure for $\tilde{z} = h$:

$$\sigma^M_{zzt} = -\bar{\alpha}\frac{C^M_{13}}{H_{\alpha t}}U^M_t + \frac{C^M_{13}}{H_{\alpha t}R_\alpha}W^M_t - \bar{\beta}\frac{C^M_{23}}{H_{\beta t}}V^M_t + \frac{C^M_{23}}{H_{\beta t}R_\beta}W^M_t + C^M_{33}W^M_{t,z} = P^M_{zt}\,, \tag{66}$$

$$\sigma^M_{\beta zt} = \bar{\beta}\frac{C^M_{44}}{H_{\beta t}}W^M_t + C^M_{44}V^M_{t,z} - \frac{C^M_{44}}{H_{\beta t}R_\beta}V^M_t = P^M_{\beta t}\,, \tag{67}$$

$$\sigma^M_{\alpha zt} = \bar{\alpha}\frac{C^M_{55}}{H_{\alpha t}}W^M_t + C^M_{55}U^M_{t,z} - \frac{C^M_{55}}{H_{\alpha t}R_\alpha}U^M_t = P^M_{\alpha t}\,, \tag{68}$$

M indicates the last layer at the top of the whole structure. Each physical layer k has been divided in q mathematical layers with constant thickness h_q. In this way total j mathematical layers have been obtained, the index j goes from 1 at the bottom to the total number M at the top. N_L indicates the number of real physical layers. Eqs.(63)-(65) written at the the bottom (b) of the first $j = 1$ layer use the conditions summarized by Eq.(57) with R_α, R_β, $\bar{\alpha}$ and $\bar{\beta}$ evaluated at the mid-surface Ω_0 of the shell, and with H^b_α and H^b_β defined at bottom of the whole structure for $\tilde{z} = 0$:

$$\sigma^1_{zzb} = -\bar{\alpha}\frac{C^1_{13}}{H_{\alpha b}}U^1_b + \frac{C^1_{13}}{H_{\alpha b}R_\alpha}W^1_b - \bar{\beta}\frac{C^1_{23}}{H_{\beta b}}V^1_b + \frac{C^1_{23}}{H_{\beta b}R_\beta}W^1_b + C^1_{33}W^1_{b,z} = P^1_{zb}\,, \tag{69}$$

$$\sigma^1_{\beta zb} = \bar{\beta}\frac{C^1_{44}}{H_{\beta b}}W^1_b + C^1_{44}V^1_{b,z} - \frac{C^1_{44}}{H_{\beta b}R_\beta}V^1_b = P^1_{\beta b}\,, \tag{70}$$

$$\sigma^1_{\alpha zb} = \bar{\alpha}\frac{C^1_{55}}{H_{\alpha b}}W^1_b + C^1_{55}U^1_{b,z} - \frac{C^1_{55}}{H_{\alpha b}R_\alpha}U^1_b = P^1_{\alpha b}\,. \tag{71}$$

Eqs.(66)-(68) in matrix form are ($\boldsymbol{U}^M(h^M)$ is vector $\boldsymbol{U}$ evaluated at the top of the whole multilayered shell, last M layer with $\tilde{z}^M = h^M$):

$$\begin{bmatrix} -\bar{\alpha}\frac{C^M_{13}}{H_{\alpha t}} & -\bar{\beta}\frac{C^M_{23}}{H_{\beta t}} & (\frac{C^M_{13}}{H_{\alpha t}R_\alpha} + \frac{C^M_{23}}{H_{\beta t}R_\beta}) & 0 & 0 & C^M_{33} \\ 0 & -\frac{C^M_{44}}{H_{\beta t}R_\beta} & \bar{\beta}\frac{C^M_{44}}{H_{\beta t}} & 0 & C^M_{44} & 0 \\ -\frac{C^M_{55}}{H_{\alpha t}R_\alpha} & 0 & \bar{\alpha}\frac{C^M_{55}}{H_{\alpha t}} & C^M_{55} & 0 & 0 \end{bmatrix} \begin{bmatrix} U^M(h^M) \\ V^M(h^M) \\ W^M(h^M) \\ U^{M\prime}(h^M) \\ V^{M\prime}(h^M) \\ W^{M\prime}(h^M) \end{bmatrix} = \begin{bmatrix} P^M_{zt} \\ P^M_{\beta t} \\ P^M_{\alpha t} \end{bmatrix}\,. \tag{72}$$

Eqs.(69)-(71) in matrix form are ($\boldsymbol{U}^1(0)$ is vector $\boldsymbol{U}$ calculated at the bottom of the whole multilayered

shell, first layer 1 with $\tilde{z}^1 = 0$):

$$\begin{bmatrix} -\bar{\alpha}\frac{C^1_{13}}{H_{\alpha b}} & -\bar{\beta}\frac{C^1_{23}}{H_{\beta b}} & (\frac{C^1_{13}}{H_{\alpha b}R_\alpha} + \frac{C^1_{23}}{H_{\beta b}R_\beta}) & 0 & 0 & C^1_{33} \\ 0 & -\frac{C^1_{44}}{H_{\beta b}R_\beta} & \bar{\beta}\frac{C^1_{44}}{H_{\beta b}} & 0 & C^1_{44} & 0 \\ -\frac{C^1_{55}}{H_{\alpha b}R_\alpha} & 0 & \bar{\alpha}\frac{C^1_{55}}{H_{\alpha b}} & C^1_{55} & 0 & 0 \end{bmatrix} \begin{bmatrix} U^1(0) \\ V^1(0) \\ W^1(0) \\ U^{1\prime}(0) \\ V^{1\prime}(0) \\ W^{1\prime}(0) \end{bmatrix} = \begin{bmatrix} P^1_{zb} \\ P^1_{\beta b} \\ P^1_{\alpha b} \end{bmatrix} . \tag{73}$$

Eqs.(72) and (73) in compact writing, to define the stress state and the loading conditions at the top and bottom of the whole structure, are:

$$\boldsymbol{B}^M(h^M)\ \boldsymbol{U}^M(h^M) = \boldsymbol{P}^M_t\,, \tag{74}$$

$$\boldsymbol{B}^1(0)\ \boldsymbol{U}^1(0) = \boldsymbol{P}^1_b\,, \tag{75}$$

with

$$\boldsymbol{P}^M_t = \begin{bmatrix} P^M_{zt} \\ P^M_{\beta t} \\ P^M_{\alpha t} \end{bmatrix}\,, \quad \boldsymbol{P}^1_b = \begin{bmatrix} P^1_{zb} \\ P^1_{\beta b} \\ P^1_{\alpha b} \end{bmatrix}\,. \tag{76}$$

In the cases proposed in the present paper, only loads in z direction applied at the top or at the bottom will be considered. Therefore, $P^M_{\beta t} = P^M_{\alpha t} = P^1_{\beta b} = P^1_{\alpha b} = 0$. This choice is made for the sake of brevity, further results with loads applied at the top and at the bottom in α and β directions will be proposed in future companion papers. Eq.(56) can be introduced in Eq.(74) for a total number of layers equals M:

$$\boldsymbol{B}^M(h^M)\ \boldsymbol{H}_m\ \boldsymbol{U}^1(0) = \boldsymbol{P}^M_t\,, \tag{77}$$

$$\boldsymbol{B}^1(0)\ \boldsymbol{U}^1(0) = \boldsymbol{P}^1_b\,, \tag{78}$$

Eqs.(77) and (78) can be grouped in a general system:

$$\begin{bmatrix} \boldsymbol{B}^M(h^M)\ \boldsymbol{H}_m \\ \boldsymbol{B}^1(0) \end{bmatrix}\ \boldsymbol{U}^1(0)\ =\ \boldsymbol{P}\ , \tag{79}$$

where the 6×6 $\boldsymbol{E}$ matrix is:

$$\boldsymbol{E}\ = \begin{bmatrix} \boldsymbol{B}^M(h^M)\ \boldsymbol{H}_m \\ \boldsymbol{B}^1(0) \end{bmatrix}\,, \tag{80}$$

and the 6×1 unknown vector $\boldsymbol{U}^1(0)$ and load vector $\boldsymbol{P}$ are:

$$\boldsymbol{U}^1(0)\ = \begin{bmatrix} U^1(0) \\ V^1(0) \\ W^1(0) \\ U^{1\prime}(0) \\ V^{1\prime}(0) \\ W^{1\prime}(0) \end{bmatrix}\,, \qquad \boldsymbol{P}\ = \begin{bmatrix} P^M_{zt} \\ 0 \\ 0 \\ P^1_{zb} \\ 0 \\ 0 \end{bmatrix}\,. \tag{81}$$

The final linear algebraic system to be solved is:

$$\boldsymbol{E}\quad \boldsymbol{U}^1(0)\ =\ \boldsymbol{P}\ . \tag{82}$$

The Eq.(82) is also valid for multilayered plate geometries without fictitious layers where $\boldsymbol{B}^{N_L}(h^{N_L}) = \boldsymbol{B}^M(h^M)$. The method always uses a layer-wise definition and the matrix $\boldsymbol{E}$ has always a 6×6 dimension, independently from the number of employed layers M. The solution is obtained via an in-house

academic software called *3DES* which has been implemented by the author in a Matlab environment. Only spherical panel equations have been implemented because they automatically degenerate into cylindrical open/closed shell and plate equations.

From the solution of Eq.(82), the vector $\boldsymbol{U}^1(0)$ is obtained. It contains the three displacement components at the bottom of the structure and their relative derivatives made with respect z. From these six values at the bottom, the 6×1 vector $\boldsymbol{U}$ can be calculated at each value of the thickness coordinate z using Eqs.(50)-(56). Strain components and stress components can be evaluated at each value of the thickness coordinate z using Eqs.(5)-(10) and (17)-(22), respectively. The proposed method is very accurate in the calculation of displacement components because it always uses a layer-wise approach even if a large number of mathematical layers is employed. The strains are calculated in an accurate way through the thickness because in Eqs.(5)-(10) the derivatives of displacements with respect to α and β are exactly obtained simply using the harmonic forms, and the derivatives of displacements with respect to z are directly obtained from the system in Eq.(82) (there is not need to numerically derive the displacements with respect to z). In this sense, this solution uses the same principle employed by mixed methods. Exact evaluations of strains through z direction in Eqs.(5)-(10) give exact evaluations of stresses through z direction by means of Eqs.(17)-(22).

3 Results

The present section is divided in two main parts. The first part proposes a validation of the model using several comparisons with other 3D solutions for plates and shells in the literature. This part is also useful to understand the number of mathematical layers M and the order of expansion N in the exponential matrix to use for a stable and correct solution. The second part proposes new benchmarks to use for future comparisons with further 2D and 3D numerical and exact models and to understand the 3D behavior of different one-layered, multilayered, sandwich and laminated structures.

3.1 Preliminary assessments

The five proposed assessments are summarized, as geometry, lamination scheme and load applications, in Table 1. The material data of the five proposed cases are shown in Table 2. Cases 1 and 2 have been proposed by Pagano in [2] for the exact 3D solution of a simply supported rectangular composite laminated plate and for a simply supported square sandwich plate, respectively. Results have been proposed in Tables 3 and 4 in terms of no-dimensional stresses and displacements:

$$(\bar{\sigma}_{\alpha\alpha}, \bar{\sigma}_{\beta\beta}, \bar{\sigma}_{\alpha\beta}) = \frac{(\sigma_{\alpha\alpha}, \sigma_{\beta\beta}, \sigma_{\alpha\beta})}{\hat{p}_z (a/h)^2}\,, \quad (\bar{\sigma}_{\alpha z}, \bar{\sigma}_{\beta z}) = \frac{(\sigma_{\alpha z}, \sigma_{\beta z})}{\hat{p}_z (a/h)}\,, \quad (\bar{w}) = \frac{100 E_2^{comp} w}{\hat{p}_z h (a/h)^4}\,. \tag{83}$$

The case 3 has been proposed by Ren [26] for the exact 3D solution of a simply supported composite laminated cylindrical shell. Results have been proposed in Table 5 in terms of no-dimensional stresses and displacements:

$$(\bar{\sigma}_{\alpha\alpha}, \bar{\sigma}_{\beta\beta}) = \frac{(\sigma_{\alpha\alpha}, \sigma_{\beta\beta})}{\hat{p}_z (R_\alpha/h)^2}\,, \quad (\bar{\sigma}_{\alpha z}) = \frac{(\sigma_{\alpha z})}{\hat{p}_z (R_\alpha/h)}\,, \quad (\bar{w}) = \frac{10 E_2^{comp} w}{\hat{p}_z h (R_\alpha/h)^4}\,. \tag{84}$$

The case 4 has been proposed by Varadan and Bhaskar [27] for the exact 3D solution of a simply supported composite laminated cylinder. Results have been proposed in Tables 6 in terms of no-dimensional stresses and displacements:

$$(\bar{\sigma}_{\alpha\alpha}, \bar{\sigma}_{\beta\beta}, \bar{\sigma}_{\alpha\beta}) = \frac{10(-\sigma_{\alpha\alpha}, -\sigma_{\beta\beta}, \sigma_{\alpha\beta})}{\hat{p}_z (R_\alpha/h)^2}\,, \quad (\bar{\sigma}_{\alpha z}, \bar{\sigma}_{\beta z}) = \frac{10(\sigma_{\alpha z}, -\sigma_{\beta z})}{\hat{p}_z (R_\alpha/h)}\,, \quad (\bar{w}) = -\frac{10 E_1^{comp} w}{\hat{p}_z h (R_\alpha/h)^4}\,, \tag{85}$$

$$\bar{\sigma}_{zz} = -\sigma_{zz}\,.$$

The case 5 has been proposed by Fan and Zhang [45] for the exact three-dimensional solution of a simply supported composite laminated spherical shell. Results have been proposed in Table 7 using the no-dimensional transverse displacement:

$$(\bar{w}) = \frac{10^3 E_2^{comp} h^3 w}{\hat{p}_z a^4}. \tag{86}$$

The present 3D exact solution has been employed in Tables 3-7 using an order of expansion $N = 3$ for the exponential matrix. $M = 102$ mathematical layers have been used for the cases 1, 4 and 5, where three layers with the same thickness have been embedded. $M = 100$ mathematical layers have been set for cases 2 and 4 for the sandwich configuration and for the two-layered shell, respectively. These choices have always guaranteed an optimal convergence of the solution and a perfect correspondence with the other proposed 3D exact solutions. For these reasons, these values will be also used in the next part where new benchmarks will be proposed.

Table 3 presents the comparison between the present 3D exact solution and the 3D exact solution by Pagano [2] for a simply-supported rectangular composite laminated plate. Transverse normal displacement, in-plane normal, in-plane shear and transverse shear stresses are given in terms of maximum amplitude (in parentheses are indicated the α and β coordinates where they are evaluated) at different z coordinates (which can vary from the bottom $-h/2$ to the top $+h/2$). In the case of quantities evaluated at interfaces, it is specified if the top or the bottom of the interface is considered. Results are given for thick and thin plates (from thickness ratio $a/h = 2$ to $a/h = 100$). The two methods are perfectly coincident for each thickness ratio and investigated variable.

Table 4 proposes the 3D exact solution by Pagano [2] and the present 3D exact method in the case of a simply-supported square sandwich plate. Comparisons have been performed for several in-plane normal/shear and transverse shear stresses evaluated as maximum amplitude at different thickness locations. Both thick and thin plates are investigated. The two methods are almost coincident for moderately thin and thin plates. Important differences are shown for thick plates. The 3D solution by Pagano [2] seems to have some problems for thick plates with an high value of transverse anisotropy (typical of sandwich structures where there is an important difference between skins and core in terms of elastic properties). The present author has verified these results adding DiQuMASPAB results which confirm the stress values by Brischetto and not those by Pagano for thickness ratios a/h equal 2, 4 and 10. Readers interested to this topic can verify this feature by means of their models. DiQuMASPAB results have been supplied by the courtesy of Dr. Tornabene and Dr. Fantuzzi using the in-house academic software DiQuMASPAB [71] based on a refined quasi-3D layer-wise model [72], [73].

Table 5 makes a comparison between the present three-dimensional exact model and that by Ren [26] for a composite laminated cylindrical shell panel. This comparison is proposed for in-plane normal and transverse shear stresses and for the transverse displacement. Such variables are evaluated as maximum amplitudes in particular positions through the thickness. For all the thickness ratios proposed (from thick structures with $R_\alpha/h = 2$ to thin structures with $R_\alpha/h = 500$), the two methods are always perfectly coincident.

Table 6 shows the results for a simply-supported composite laminated cylinder. 3D solution by Varadan and Bhaskar [27] is compared with the present 3D exact method in terms of transverse displacement and in-plane and transverse shear/normal stresses. All the quantities are investigated in terms of maximum amplitudes through different thickness positions. The two models are always perfectly coincident for each thickness ratio R_α/h proposed.

The last Table 7 proposes the comparison between the present three-dimensional exact model and that by Fan and Zhang [45] for the analysis of a composite multilayered spherical panel in terms of no-dimensional transverse displacement $\bar{w}$ evaluated in the middle of the structure. The two solutions are coincident for each thickness ratio h/R_α.

3.2 New benchmarks

The present 3D exact shell solution, validated in the previous part, is here used to propose new benchmarks. From the previous verifications, the proposed 3D shell model can be used with confidence by means of an order of expansion $N = 3$ for the exponential matrix. $N = 100$ mathematical layers are used for one-layered, two-layered and sandwich configurations. $N = 102$ mathematical layers are used for three-layered structures with the same thickness for the three layers. New proposed benchmarks are important for two main reasons. They can be used for a complete validation of new refined 2D and 3D shell models proposed in the literature because they propose a large variety of geometries, lamination schemes and employed materials. Moreover, they allow to investigate typical three-dimensional effects and 3D behaviors which are typical of high thickness values and high values of transverse and in-plane anisotropy.

Benchmark 1 considers a one-layered isotropic square plate. Benchmark 2 proposes a two-layered rectangular plate embedding two different isotropic layers with the same thickness. Benchmark 3 investigates a three-layered cylinder embedding three different isotropic layers with the same thickness. Benchmark 4 shows a sandwich cylindrical shell panel with two external isotropic skins and an internal soft core. The last benchmark, the number 5, considers a three-layered composite cross-ply $(0°/90°/0°)$ spherical shell panel. All the five structures are simply-supported and subjected to a mechanical load applied at the top in harmonic form with half-wave numbers m, n as indicated in Table 8 and amplitude $P_z = 1Pa$. All the geometrical, lamination and load features of the five proposed benchmarks are summarized in Figure 2 and Table 8. Table 9 contains the elastic properties of all the materials employed in the five proposed benchmarks. Tables 10-14 and Figures 3-8 show the results for the five proposed benchmarks using no-dimensional displacements and stresses. No-dimensional forms for benchmarks 1 and 2 are:

$$(\bar{u}, \bar{v}, \bar{w}) = \frac{10^2 E_2^{bottom}(u, v, w)}{\hat{p}_z h (a/h)^4}, \quad (\bar{\sigma}_{\alpha\alpha}, \bar{\sigma}_{\beta\beta}, \bar{\sigma}_{\alpha\beta}) = \frac{(\sigma_{\alpha\alpha}, \sigma_{\beta\beta}, \sigma_{\alpha\beta})}{\hat{p}_z (a/h)^2}, \tag{87}$$

$$(\bar{\sigma}_{\alpha z}, \bar{\sigma}_{\beta z}) = \frac{(\sigma_{\alpha z}, \sigma_{\beta z})}{\hat{p}_z (a/h)}, \quad \bar{\sigma}_{zz} = \sigma_{zz}.$$

No-dimensional forms for benchmarks 3, 4 and 5 are:

$$(\bar{u}, \bar{v}, \bar{w}) = \frac{10^4 E_2^{bottom}(u, v, w)}{\hat{p}_z h (R_\alpha/h)^4}, \quad (\bar{\sigma}_{\alpha\alpha}, \bar{\sigma}_{\beta\beta}, \bar{\sigma}_{\alpha\beta}) = \frac{10^3(\sigma_{\alpha\alpha}, \sigma_{\beta\beta}, \sigma_{\alpha\beta})}{\hat{p}_z (R_\alpha/h)^2}, \tag{88}$$

$$(\bar{\sigma}_{\alpha z}, \bar{\sigma}_{\beta z}) = \frac{10^3(\sigma_{\alpha z}, \sigma_{\beta z})}{\hat{p}_z (R_\alpha/h)}, \quad \bar{\sigma}_{zz} = \sigma_{zz}.$$

Tables 10-14 propose the no-dimensional forms of the three displacement components and the six stress components in terms of maximum amplitude. They are evaluated at the top, middle and bottom of the structure. When the middle surface coincides with a physical interface (e.g., Table 11), the top of the first layer is considered. Results in Tables 10-14 are proposed for thick and thin structures (thickness ratios from $a/h = 2$ to $a/h = 100$ for plates and from $R_\alpha/h = 2$ to $R_\alpha/h = 500$ for shells). Displacements proposed in Figure 3 and stresses evaluated in Figures 4-8 for all the five benchmarks are given as no-dimensional quantities through the thickness direction in terms of maximum amplitudes.

Benchmark 1 is proposed in Table 10. The one-layered isotropic square plate has a symmetric behavior in the plane in fact $\bar{u} = \bar{v}$, $\bar{\sigma}_{\alpha\alpha} = \bar{\sigma}_{\beta\beta}$ and $\bar{\sigma}_{\alpha z} = \bar{\sigma}_{\beta z}$. The symmetric behavior through the thickness is possible only for thin and moderately thin structure, in fact for thickness ratios greater than $a/h = 20$ the top displacement values and the bottom displacement values are equal and the same feature is shown for in-plane and transverse shear stresses. Transverse shear stresses $\bar{\sigma}_{\alpha z}$ and $\bar{\sigma}_{\beta z}$ are equal to 0 at the top and at the bottom of the structure because no P_α and P_β loads have been

applied. Transverse normal stress $\bar{\sigma}_{zz}$ is equal to 1 at the top and equals 0 at the bottom because a load $P_z = 1Pa$ has been applied at the top of the structure. The first image of Figure 3 for a thick plate confirms the displacement behavior through the thickness direction. Figure 4 shows the six stress components through the thickness of a thick plate, all the considerations obtained by means of the table results are here confirmed.

Benchmark 2 is analyzed in Table 11. The two-layered isotropic rectangular plate does not have a symmetric behavior in the plane because the two sides are different ($a = 3b$), in fact $\bar{u} \neq \bar{v}$, $\bar{\sigma}_{\alpha\alpha} \neq \bar{\sigma}_{\beta\beta}$ and $\bar{\sigma}_{\alpha z} \neq \bar{\sigma}_{\beta z}$. The symmetric behavior through the thickness is not possible even if the structure is very thin ($a/h = 100$) because there is an important transverse anisotropy due to the presence of two different isotropic layers with large differences in terms of elastic properties. For this reason, top displacement values are different from bottom displacement values, and top in-plane stresses are different from bottom in-plane stresses for each thickness ratio. It is confirmed that transverse shear stresses $\bar{\sigma}_{\alpha z}$ and $\bar{\sigma}_{\beta z}$ are equal to 0 at the top and at the bottom of the structure because no P_α and P_β loads have been applied. Transverse normal stress $\bar{\sigma}_{zz}$ is equal to 1 at the top and equals 0 at the bottom because a load $P_z = 1Pa$ is applied at the top of the structure. The second image of Figure 3 for a thick plate confirms the displacement behavior through the thickness direction. Displacements are continuous through the interface between the two layers because the compatibility conditions have been imposed in the proposed 3D shell model. Figure 5 gives the six stress components through the thickness for a thick plate. All the considerations obtained by means of table results are here confirmed. Transverse shear and transverse normal stresses must be continuous through the thickness and at the interface between the two layers because of equilibrium reasons. In-plane normal and in-plane shear stresses can be discontinuous at the interface as demonstrated in the first three images. All these conditions have been successfully included in the employed 3D layer-wise shell model.

Benchmark 3 is studied in Table 12. The three-layered isotropic cylinder does not have a symmetry in terms of variables $\bar{u}$, $\bar{v}$, $\bar{\sigma}_{\alpha\alpha}$, $\bar{\sigma}_{\beta\beta}$, $\bar{\sigma}_{\alpha z}$ and $\bar{\sigma}_{\beta z}$. The symmetric behavior is also not present in the thickness direction because of the three different isotropic layers with different elastic properties which give an important transverse anisotropy. This feature is confirmed for all the thickness ratios, even if displacements become constant through the thickness for the $R_\alpha/h = 500$ case. Top in-plane stresses are different from bottom in-plane stresses for each thickness ratio. Transverse shear stresses are zero at the top and at the bottom to satisfy the loading boundary conditions ($P_\alpha = P_\beta = 0$). Transverse normal stress is zero at the bottom and equals 1 at the top because the transverse normal load P_z is zero at the bottom and equals 1Pa at the top, respectively. The third image of Figure 3 gives an exhaustive evaluation of the three displacement components through the thickness of a very thick three-layered cylinder. All the three displacement components are continuous through the two interfaces because the compatibility conditions have been satisfied in the proposed 3D shell model. Figure 6 gives the six stress components through the thickness of a thick three-layered cylinder confirming the results seen in Table 12. Transverse shear and transverse normal stresses must be continuous through the thickness and at the two interfaces because of imposed equilibrium conditions. In-plane normal and in-plane shear stresses can be discontinuous at the interfaces as demonstrated in the first three images of Figure 6. All these conditions are clearly given in the proposed figure because compatibility and equilibrium conditions have been correctly imposed in the 3D shell model. The proposed model uses a layer-wise approach and this feature is clearly demonstrated in Figure 6 where the typical zigzag form is shown. This behavior is due to the high transverse anisotropy connected with the presence of three different isotropic layers.

Table 13 proposes the benchmark 4 for the sandwich cylindrical shell panel. The investigated variables demonstrate the absence of symmetry in the in-plane direction and in the behavior through the thickness direction z. These features are connected with the absence of symmetry in the geometry and with the presence of a soft core. When a load is applied at the top of the structure, such load effects are not completely transferred to the bottom skin because of the presence of a very soft central

core. Loading boundary conditions ($P_\alpha = P_\beta = 0$ at both top and bottom surfaces, and $P_z = 0$ at the bottom and $P_z = 1Pa$ at the top) are satisfied. For these reasons, transverse shear stresses $\bar{\sigma}_{\alpha z}$ and $\bar{\sigma}_{\beta z}$ are zero at both external surfaces, and transverse normal stress $\bar{\sigma}_{zz}$ is zero at the bottom of the structure and equals 1 at the top. The fourth image of Figure 3 shows a clear zigzag behavior through the thickness for the three displacement components. In fact, in this case the transverse anisotropy is very large because of the presence of a very soft central core. The proposed layer-wise 3D shell model captures this behavior and the displacements remain continuous through the thickness because of the opportune imposition of the compatibility conditions in the model. Figure 7 shows the six stress components through the thickness direction of a thick shell. The presence of two external thin skins, with a rigidity larger than the core rigidity, and an internal very soft core with a thickness equals 0.8 times the total thickness of the structure is clearly shown. The zigzag affect and the presence of the two interfaces between the skins and the core are clearly demonstrated. In-plane stresses are discontinuous at each physical interface. On the contrary, transverse stresses are continuous because of the imposed equilibrium conditions. The transverse stresses clearly confirm the imposed external loading conditions. The 3D behavior of such structures is clearly evaluated by the present model and it must be reproduced by those 2D refined theories developed for these types of investigation.

The last benchmark 5 concerns the cross-ply three-layered composite spherical shell panel. The main results are proposed in Table 14. Even if the structure has a geometrical symmetry, the presence of three composite layers with lamination scheme $0°/90°/0°$ gives differences between $\bar{u}$ and $\bar{v}$, $\bar{\sigma}_{\alpha\alpha}$ and $\bar{\sigma}_{\beta\beta}$, and $\bar{\sigma}_{\alpha z}$ and $\bar{\sigma}_{\beta z}$. There is not a symmetrical behavior through the thickness because of the transverse and in-plane anisotropy combined with the complicated geometry of the structure (the presence of two radii of curvature). For very thin shells, displacements are constant through the thickness. Transverse shear and transverse normal stresses correctly satisfy the boundary loading conditions. The fifth image of Figure 3 confirms the typical zigzag form of displacements (in particular for thick shells) which can be recovered by means of the proposed 3D shell model because it is based on a layer wise approach. Displacements are continuous through the thickness direction and at each physical interface. The six stress component behavior through the thickness direction is described in Figure 8 for the case of a very thick spherical shell. The in-plane normal stresses are discontinuous through the thickness and they do not have any symmetry. Transverse shear and transverse normal stresses are continuous and they reflect the loading boundary conditions. Their non-symmetric behavior is clearly shown, in particular for the $\bar{\sigma}_{\beta z}$ stress. The three-dimensional behavior of such a structure is clearly shown and it is due to the lamination scheme, presence of orthotropic materials, thickness ratio and geometry.

4 Conclusions

This work has presented an exact 3D shell model for the static analysis of simply supported plates and shells subjected to a transverse normal load applied at the top in harmonic form. The method is based on the three-dimensional shell equilibrium equations developed in a general orthogonal curvilinear reference system. These equations, valid for spherical shells, easily degenerate in those for cylinders, cylindrical shells and plates. For these reasons, the method is very general and it has been employed to investigate square plates, rectangular plates, cylinders, cylindrical shells and spherical shells. Such geometries can be one-layered or multilayered embedding isotropic, orthotropic or composite materials (also including laminated and sandwich configurations). The proposed equations have been proposed in closed form using simply supported boundary conditions and harmonic forms for displacements, stresses and loads. The differential equations in z have been solved using the exponential matrix procedure which has been successfully employed by the same author in his past works for the free vibration analysis. The model uses a layer wise approach and it directly imposes the compatibility conditions for displacements, the equilibrium conditions for the transverse stresses and the loading conditions for the applied loads. For all these reasons, the method is very accurate for each geometry, lamination

scheme, material and thickness ratio. It always gives a complete three-dimensional description of all displacement and stress components, and it allows the inclusion of all the three-dimensional effects such as the transverse and in-plane anisotropy and the consequent zigzag behavior of displacements. Such results can be employed as reference solutions by those scientists involved in the development of new 3D and refined 2D numerical shell models.

References

[1] N.J. Pagano, Exact solutions for composite laminates in cylindrical bending, *Journal of Composite Materials*, 3, 398-411, 1969.

[2] N.J. Pagano, Exact solutions for rectangular bidirectional composites and sandwich plates, *Journal of Composite Materials*, 4, 20-34, 1970.

[3] N.J. Pagano and A.S.D. Wang, Further study of composite laminates under cylindrical bending, *Journal of Composite Materials*, 5, 521-528, 1971.

[4] L. Demasi, Three-dimensional closed form solutions and exact thin plate theories for isotropic plates, *Composite Structures*, 80, 183-195, 2007.

[5] S. Aimmanee and R.C. Batra, Analytical solution for vibration of an incompressible isotropic linear elastic rectangular plate, and frequencies missed in previous solutions, *Journal of Sound and Vibration*, 302, 613-620, 2007.

[6] R.C. Batra and S. Aimmanee, Letter to the Editor: Missing frequencies in previous exact solutions of free vibrations of simply supported rectangular plates, *Journal of Sound and Vibration*, 265, 887-896, 2003.

[7] S. Srinivas, C.V.J. Rao and A.K. Rao, An exact analysis for vibration of simply-supported homogeneous and laminated thick rectangular plates, *Journal of Sound and Vibration*, 12, 187-199, 1970.

[8] S. Srinivas, A.K. Rao and C.V.J. Rao, Flexure of simply supported thick homogeneous and laminated rectangular plates, *Zeitschrift für Angewandte Mathematik und Mechanik*, 49, 449-458, 1969.

[9] R.C. Batra, S. Vidoli and F. Vestroni, Plane wave solutions and modal analysis in higher order shear and normal deformable plate theories, *Journal of Sound and Vibration*, 257, 63-88, 2002.

[10] J.Q. Ye, A three-dimensional free vibration analysis of cross-ply laminated rectangular plates with clamped edges, *Computer Methods in Applied Mechanics and Engineering*, 140, 383-392, 1997.

[11] A. Messina, Three dimensional free vibration analysis of cross-ply laminated plates through 2D and exact models, *3rd International Conference on Integrity, Reliability and Failure*, Porto (Portugal), 20-24 July 2009.

[12] Y.K. Cheung and D. Zhou, Three-dimensional vibration analysis of cantilevered and completely free isosceles triangular plates, *International Journal of Solids and Structures*, 39, 673-687, 2002.

[13] K.M. Liew and B. Yang, Three-dimensional elasticity solutions for free vibrations of circular plates: a polynomials-Ritz analysis, *Computer Methods in Applied Mechanics and Engineering*, 175, 189-201, 1999.

[14] H. Rokni Damavandi Taher, M. Omidi, A.A. Zadpoor and A.A. Nikooyan, Short Communication: Free vibration of circular and annular plates with variable thickness and different combinations of boundary conditions, *Journal of Sound and Vibration*, 296, 1084-1092, 2006.

[15] Y. Xing and B. Liu, New exact solutions for free vibrations of rectangular thin plates by symplectic dual method, *Acta Mechanica Sinica*, 25, 265-270, 2009.

[16] Sh. Hosseini-Hashemi, H. Salehipour and S.R. Atashipour, Exact three-dimensional free vibration analysis of thick homogeneous plates coated by a functionally graded layer, *Acta Mechanica*, 223, 2153-2166, 2012.

[17] S.S. Vel and R.C. Batra, Three-dimensional exact solution for the vibration of functionally graded rectangular plates, *Journal of Sound and Vibration*, 272, 703-730, 2004.

[18] Y. Xu and D. Zhou, Three-dimensional elasticity solution of functionally graded rectangular plates with variable thickness, *Composite Structures*, 91, 56-65, 2009.

[19] D. Haojiang, X. Rongqiao and C. Weiqiu, Exact solutions for free vibration of transversely isotropic piezoelectric circular plates, *Acta Mechanica Sinica*, 16, 142-147, 2000.

[20] B.P. Baillargeon and S.S. Vel, Exact solution for the vibration and active damping of composite plates with piezoelectric shear actuators, *Journal of Sound and Vibration*, 282, 781-804, 2005.

[21] W.Q. Chen, J.B. Cai, G.R. Ye and Y.F. Wang, Exact three-dimensional solutions of laminated orthotropic piezoelectric rectangular plates featuring interlaminar bonding imperfections modeled by a general spring layer, *International Journal of Solids and Structures*, 41, 5247-5263, 2004.

[22] Z.-Q. Cheng, C.W. Lim and S. Kitipornchai, Three-dimensional exact solution for inhomogeneous and laminated piezoelectric plates, *International Journal of Engineering Science*, 37, 1425-1439, 1999.

[23] S. Kapuria and P.G. Nair, Exact three-dimensional piezothermoelasticity solution for dynamics of rectangular cross-ply hybrid plates featuring interlaminar bonding imperfections, *Composites Science and Technology*, 70, 752-762, 2010.

[24] Z. Zhong and E.T. Shang, Three-dimensional exact analysis of a simply supported functionally gradient piezoelectric plate, *International Journal of Solids and Structures*, 40, 5335-5352, 2003.

[25] H.-R. Meyer-Piening, Application of the elasticity solution to linear sandwich beam, plate and shell analyses, *Journal of Sandwich Structures and Materials*, 6, 295-312, 2004.

[26] J.G. Ren, Exact solutions for laminated cylindrical shells in cylindrical bending, *Composite Science and Technology*, 29, 169-187, 1987.

[27] T.K. Varadan and K. Bhaskar, Bending of laminated orthotropic cylindrical shells - an elasticity approach, *Composite Structures*, 17, 141-156, 1991.

[28] W.-Q. Chen, H.-J. Ding and R.-Q. Xu, On exact analysis of free vibrations of embedded transversely isotropic cylindrical shells, *International Journal of Pressure Vessels and Piping*, 75, 961-966, 1998.

[29] J.-R. Fan and J.-Y. Zhang, Exact solutions for thick laminated shells, *Science in China*, 35, 1343-1355, 1992.

[30] B. Gasemzadeh, R. Azarafza, Y. Sahebi and A. Motallebi, Analysis of free vibration of cylindrical shells on the basis of three dimensional exact elasticity theory, *Indian Journal of Science and Technology*, 5, 3260-3262, 2012.

[31] N.N. Huang, Exact analysis for three-dimensional free vibrations of cross-ply cylindrical and doubly-curved laminates, *Acta Mechanica*, 108, 23-34, 1995.

[32] J.N. Sharma, D.K. Sharma and S.S. Dhaliwal, Three-dimensional free vibration analysis of a viscothermoelastic hollow sphere, *Open Journal of Acoustics*, 2, 12-24, 2012.

[33] J.N. Sharma and N. Sharma, Three-dimensional free vibration analysis of a homogeneous transradially isotropic thermoelastic sphere, *Journal of Applied Mechanics*, 77, 1-9, 2010.

[34] K.P. Soldatos and J. Ye, Axisymmetric static and dynamic analysis of laminated hollow cylinders composed of monoclinic elastic layers, *Journal of Sound and Vibration*, 184, 245-259, 1995.

[35] A.E. Armenakas, D.C. Gazis and G. Herrmann, *Free Vibrations of Circular Cylindrical Shells*, Pergamon Press, Oxford, 1969.

[36] A. Bhimaraddi, A higher order theory for free vibration analysis of circular cylindrical shells, *International Journal of Solids and Structures*, 20, 623-630, 1984.

[37] H. Zhou, W. Li, B. Lv and W.L. Li, Free vibrations of cylindrical shells with elastic-support boundary conditions, *Applied Acoustics*, 73, 751-756, 2012.

[38] S.M.R. Khalili, A. Davar and K.M. Fard, Free vibration analysis of homogeneous isotropic circular cylindrical shells based on a new three-dimensional refined higher-order theory, *International Journal of Mechanical Sciences*, 56, 1-25, 2012.

[39] S.S. Vel, Exact elasticity solution for the vibration of functionally graded anisotropic cylindrical shells, *Composite Structures*, 92, 2712-2727, 2010.

[40] C.T. Loy and K.Y. Lam, Vibration of thick cylindrical shells on the basis of three-dimensional theory of elasticity, *Journal of Sound and Vibration*, 226, 719-737, 1999.

[41] Y. Wang, R. Xu, H. Ding and J. Chen, Three-dimensional exact solutions for free vibrations of simply supported magneto-electro-elastic cylindrical panels, *International Journal of Engineering Science*, 48, 1778-1796, 2010.

[42] E. Efraim and M. Eisenberger, Exact vibration frequencies of segmented axisymmetric shells, *Thin-Walled Structures*, 44, 281-289, 2006.

[43] J.-H. Kanga and A.W. Leissa, Three-dimensional vibrations of thick spherical shell segments with variable thickness, *International Journal of Solids and Structures*, 37, 4811-4823, 2000.

[44] K.M. Liew, L.X. Peng and T.Y. Ng, Three-dimensional vibration analysis of spherical shell panels subjected to different boundary conditions, *International Journal of Mechanical Sciences*, 44, 2103-2117, 2002.

[45] J. Fan and J. Zhang, Analytical solutions for thick, doubly curved, laminated shells, *Journal of Engineering Mechanics*, 118, 1338-1356, 1992.

[46] J. Fan and J. Ye, An exact solution for the statics and dynamics of laminated thick plates with orthotropic layers, *International Journal of Solids and Structures*, 26, 655-662, 1990.

[47] S. Brischetto, Three-dimensional exact free vibration analysis of spherical, cylindrical, and flat one-layered panels, *Shock and Vibration*, vol.2014, 1-29, 2014.

[48] S. Brischetto, An exact 3D solution for free vibrations of multilayered cross-ply composite and sandwich plates and shells, *International Journal of Applied Mechanics*, 6, 1-42, 2014.

[49] S. Brischetto, Exact elasticity solution for natural frequencies of functionally graded simply-supported structures, *Computer Modeling in Engineering & Sciences*, 95, 391-430, 2013.

[50] S. Brischetto, A continuum elastic three-dimensional model for natural frequencies of single-walled carbon nanotubes, *Composites part B: engineering*, 61, 222-228, 2014.

[51] S. Brischetto, A continuum shell model including van derWaals interaction for free vibrations of double-walled carbon nanotubes, *Computer Modeling in Engineering & Sciences*, 104, 305-327, 2015.

[52] S. Brischetto, Convergence analysis of the exponential matrix method for the solution of 3D equilibrium equations for free vibration analysis of plates and shells, *Composites part B: engineering*, 98, 453-471, 2016.

[53] S. Brischetto, Exact and approximate shell geometry in the free vibration analysis of one-layered and multilayered structures, *International Journal of Mechanical Sciences*, 113, 81-93, 2016.

[54] S. Brischetto, Curvature approximation effects in the free vibration analysis of functionally graded shells, *International Journal of Applied Mechanics*, 8, 1-33, 2016.

[55] S. Brischetto and R. Torre, Exact 3D solutions and finite element 2D models for free vibration analysis of plates and cylinders, *Curved and Layered Structures*, 1, 59-92, 2014.

[56] F. Tornabene, S. Brischetto, N. Fantuzzi and E. Viola, Numerical and exact models for free vibration analysis of cylindrical and spherical shell panels, *Composites part B: engineering*, 81, 231-250, 2015.

[57] S. Brischetto, F. Tornabene, N. Fantuzzi and M. Bacciocchi, Refined 2D and exact 3D shell models for the free vibration analysis of single- and double-walled carbon nanotubes, *Technologies*, 3, 259-284, 2015.

[58] S. Brischetto, F. Tornabene, N. Fantuzzi and E. Viola, 3D exact and 2D generalized differential quadrature models for free vibration analysis of functionally graded plates and cylinders, *Meccanica*, 51, 2059-2098, 2016.

[59] N. Fantuzzi, S. Brischetto, F. Tornabene and E. Viola, 2D and 3D shell models for the free vibration investigation of functionally graded cylindrical and spherical panels, *Composite Structures*, 154, 573-590, 2016.

[60] S. Brischetto, F. Tornabene, N. Fantuzzi and M. Bacciocchi, Interpretation of boundary conditions in the analytical and numerical shell solutions for mode analysis of multilayered structures, *International Journal of Mechanical Sciences*, 122, 18-28, 2017.

[61] F. Tornabene, S. Brischetto, N. Fantuzzi and M. Bacciocchi, Boundary conditions in 2D numerical and 3D exact models for cylindrical bending analysis of functionally graded structures, *Shock and Vibration*, vol.2016, 1-17, 2016.

[62] A.W. Leissa, *Vibration of Plates*, NASA SP-160, Washington, 1969.

[63] A.W. Leissa, *Vibration of Shells*, NASA SP-288, Washington, 1973.

[64] W. Soedel, *Vibration of Shells and Plates*, Marcel Dekker, Inc., New York, 2004.

[65] F.B. Hildebrand, E. Reissner and G.B. Thomas, *Notes on the Foundations of the Theory of Small Displacements of Orthotropic Shells*, NACA Technical Note No. 1833, Washington, 1949.

[66] F. Tornabene, *Meccanica delle Strutture a Guscio in Materiale Composito*, Societá Editrice Esculapio, Bologna (Italy), 2012.

[67] Open document, *Systems of Differential Equations*, free available on http://www.math.utah.edu/gustafso/, accessed on 30th May 2013.

[68] W.E. Boyce and R.C. DiPrima, *Elementary Differential Equations and Boundary Value Problems*, John Wiley & Sons, Ltd., New York, 2001.

[69] D. Zwillinger, *Handbook of Differential Equations*, Academic Press, New York, 1997.

[70] C. Molery and C. Van Loan, Nineteen dubious ways to compute the exponential of a matrix, twenty-five years later, *SIAM Review*, 45, 1-46, 2003.

[71] DiQuMASPAB Project, *Differential Quadrature for Mechanics of Anisotropic Shells, Plates, Arches and Beams*, free available on software.dicam.unibo.it/diqumaspab-project, accessed on 27th January 2017.

[72] F. Tornabene, N. Fantuzzi, M. Bacciocchi and E. Viola, Accurate inter-laminar recovery for plates and doubly-curved shells with variable radii of curvature using layer-wise theories, *Composite Structures*, 124, 368-393, 2015.

[73] F. Tornabene, General higher-order layer-wise theory for free vibrations of doubly-curved laminated composite shells and panels, *Mechanics of Advanced Materials and Structures*, 23, 1046-1067, 2016.

	Case 1	Case 2	Case 3	Case 4	Case 5
a[in]	1	1	$\frac{\pi}{3}R_\alpha$	$2\pi R_\alpha$	10
b[in]	3	1	1	40	10
R_α[in]	∞	∞	10	10	10
R_β[in]	∞	∞	∞	∞	10
h_1	h/3	0.1h	0.5h	h/3	h/3
h_2	h/3	0.8h	0.5h	h/3	h/3
h_3	h/3	0.1h	-	h/3	h/3
sequence	0°/90°/0°	0°/*core*/0°	90°/0°	0°/90°/0°	0°/90°/0°
$\hat{p}_z$[psi]	1(top)	1(top)	1(top)	1(bottom)	1(top)
m[-]	1	1	1	8	1
n[-]	1	1	0	1	1

Table 1: Load and geometrical data for the case 1 about the rectangular composite laminated plate proposed by Pagano [2], the case 2 about the square sandwich plate proposed by Pagano [2], the case 3 about the composite laminated cylindrical panel proposed by Ren [26], the case 4 about the composite laminated cylinder by Varadan and Bhaskar [27] and the case 5 about the composite laminated spherical panel proposed by Fan and Zhang [45].

	Composite for cases 1-5	Core material for case 2
E_1[psi]	25×10^6	0.04×10^6
E_2[psi]	1×10^6	0.04×10^6
E_3[psi]	1×10^6	0.5×10^6
G_{12}[psi]	0.5×10^6	0.016×10^6
G_{13}[psi]	0.5×10^6	0.06×10^6
G_{23}[psi]	0.2×10^6	0.06×10^6
ν_{12}	0.25	0.25
ν_{13}	0.25	0.25
ν_{23}	0.25	0.25

Table 2: Material data for the five cases proposed in Table 1.

(α,β) (z)	$\bar{\sigma}_{\alpha\alpha}$ $(\frac{a}{2},\frac{b}{2})$ $(\frac{h}{2})$	$\bar{\sigma}_{\alpha\alpha}$ $(\frac{a}{2},\frac{b}{2})$ $(-\frac{h}{2})$	$\bar{\sigma}_{\beta\beta}$ $(\frac{a}{2},\frac{b}{2})$ $(\frac{h}{6}^{*})$	$\bar{\sigma}_{\beta\beta}$ $(\frac{a}{2},\frac{b}{2})$ $(-\frac{h}{6}^{**})$	$\bar{\sigma}_{\alpha z}$ $(0,\frac{b}{2})$ (0)	$\bar{\sigma}_{\beta z}$ $(\frac{a}{2},0)$ (0)	$\bar{\sigma}_{\alpha\beta}$ $(0,0)$ $(\frac{h}{2})$	$\bar{\sigma}_{\alpha\beta}$ $(0,0)$ $(-\frac{h}{2})$	$\bar{w}$ $(\frac{a}{2},\frac{b}{2})$ (0)
					a/h=2				
3D Pagano [2]	2.13	-1.62	0.230	-0.268	0.257	0.0668	-0.0564	0.0548	8.17
Present 3D	2.13	-1.62	0.229	-0.268	0.257	0.0668	-0.0564	0.0548	8.17
					a/h=4				
3D Pagano [2]	1.14	-1.10	0.109	-0.119	0.351	0.0334	-0.0269	0.0281	2.82
Present 3D	1.14	-1.10	0.109	-0.119	0.351	0.0334	-0.0269	0.0281	2.82
					a/h=10				
3D Pagano [2]	0.726	-0.725	0.0418	-0.0435	0.420	0.0152	-0.0120	0.0123	0.919
Present 3D	0.726	-0.725	0.0418	-0.0435	0.420	0.0152	-0.0120	0.0123	0.919
					a/h=20				
3D Pagano [2]	0.650	-0.650	0.0294	-0.0299	0.434	0.0119	-0.0093	0.0093	0.610
Present 3D	0.650	-0.650	0.0294	-0.0299	0.434	0.0119	-0.0092	0.0093	0.609
					a/h=50				
3D Pagano [2]	0.628	-0.628	0.0259	-0.0259	0.439	0.0110	-0.0084	0.0084	0.520
Present 3D	0.628	-0.628	0.0258	-0.0259	0.439	0.0110	-0.0084	0.0084	0.520
					a/h=100				
3D Pagano [2]	0.624	-0.624	0.0253	-0.0253	0.439	0.0108	-0.0083	0.0083	0.508
Present 3D	0.624	-0.624	0.0253	-0.0253	0.439	0.0108	-0.0083	0.0083	0.508

Table 3: Case 1, present 3D solution compared with the 3D solution proposed by Pagano [2] for a rectangular laminated composite plate. *bottom of the second interface. ** top of the first interface.

(α,β)	$\bar{\sigma}_{\alpha\alpha}$ $(\frac{a}{2},\frac{b}{2})$	$\bar{\sigma}_{\alpha\alpha}$ $(\frac{a}{2},\frac{b}{2})$	$\bar{\sigma}_{\alpha\alpha}$ $(\frac{a}{2},\frac{b}{2})$	$\bar{\sigma}_{\alpha\alpha}$ $(\frac{a}{2},\frac{b}{2})$	$\bar{\sigma}_{\beta\beta}$ $(\frac{a}{2},\frac{b}{2})$	$\bar{\sigma}_{\beta\beta}$ $(\frac{a}{2},\frac{b}{2})$	$\bar{\sigma}_{\alpha z}$ $(0,\frac{b}{2})$	$\bar{\sigma}_{\beta z}$ $(\frac{a}{2},0)$	$\bar{\sigma}_{\alpha\beta}$ $(0,0)$	$\bar{\sigma}_{\alpha\beta}$ $(0,0)$
(z)	$(\frac{h}{2})$	$(-\frac{h}{2})$	$(0.4h^*)$	$(-0.4h^{**})$	$(\frac{h}{2})$	$(-\frac{h}{2})$	(0)	(0)	$(\frac{h}{2})$	$(-\frac{h}{2})$
					a/h=2					
3D Pagano [2]	3.278	-2.653	-2.220	1.668	0.4517	-0.3919	0.185	0.1399	-0.2403	0.2338
Present 3D	2.494	-3.100	-1.753	1.936	0.3022	-0.4892	0.192	0.1505	-0.1545	0.2886
DiQuMASPAB [71]	2.494	-3.100	-1.753	1.914	0.3022	-0.4892	0.192	0.1505	-0.1545	0.2886
					a/h=4					
3D Pagano [2]	1.556	-1.512	-0.233	0.196	0.2595	-0.2533	0.239	0.1072	-0.1437	0.1481
Present 3D	1.468	-1.543	-0.220	0.198	0.2307	-0.2730	0.240	0.1106	-0.1281	0.1583
DiQuMASPAB [71]	1.468	-1.543	-0.220	0.191	0.2307	-0.2730	0.240	0.1106	-0.1281	0.1583
					a/h=10					
3D Pagano [2]	1.153	-1.152	0.628	-0.629	0.1104	-0.1099	0.300	0.0527	-0.0707	0.0717
Present 3D	1.145	-1.153	0.623	-0.630	0.1065	-0.1131	0.300	0.0534	-0.0686	0.0733
DiQuMASPAB [71]	1.145	-1.153	0.623	-0.633	0.1065	-0.1131	0.300	0.0534	-0.0686	0.0733
					a/h=20					
3D Pagano [2]	1.110	-1.110	0.810	-0.810	0.0700	-0.0700	0.317	0.0361	-0.0511	0.0511
Present 3D	1.108	-1.110	0.808	-0.810	0.0691	-0.0708	0.317	0.0363	-0.0505	0.0517
DiQuMASPAB [71]	1.108	-1.110	0.808	-0.812	0.0691	-0.0708	0.317	0.0363	-0.0505	0.0517
					a/h=50					
3D Pagano [2]	1.099	-1.099	0.867	-0.867	0.0569	-0.0569	0.323	0.0306	-0.0446	0.0446
Present 3D	1.099	-1.099	0.866	-0.866	0.0568	-0.0570	0.323	0.0306	-0.0445	0.0447
DiQuMASPAB [71]	1.099	-1.099	0.866	-0.866	0.0568	-0.0570	0.323	0.0306	-0.0445	0.0447
					a/h=100					
3D Pagano [2]	1.098	-1.098	0.875	-0.875	0.0550	-0.0550	0.324	0.0297	-0.0437	0.0437
Present 3D	1.097	-1.097	0.875	-0.875	0.0549	-0.0550	0.324	0.0297	-0.0436	0.0437
DiQuMASPAB [71]	1.097	-1.098	0.875	-0.876	0.0549	-0.0550	0.324	0.0298	-0.0436	0.0437

Table 4: Case 2, present 3D solution compared with the 3D solution proposed by Pagano [2] for a square sandwich plate. * top of the interface between core and top skin. ** bottom of the interface between core and bottom skin. *DiQuMASPAB results have been obtained using the DiQuMASPAB code [71] based on a refined quasi-3D layer-wise model [72], [73].*

(α,β)	$\bar{w}$ $(\frac{a}{2},\frac{b}{2})$	$\bar{\sigma}_{\alpha\alpha}$ $(\frac{a}{2},\frac{b}{2})$	$\bar{\sigma}_{\alpha\alpha}$ $(\frac{a}{2},\frac{b}{2})$	$\bar{\sigma}_{\beta\beta}$ $(\frac{a}{2},\frac{b}{2})$	$\bar{\sigma}_{\beta\beta}$ $(\frac{a}{2},\frac{b}{2})$	$\bar{\sigma}_{\alpha z}$ $(0,\frac{b}{2})$
(z)	(0)	$(-\frac{h}{2})$	$(\frac{h}{2})$	$(-\frac{h}{2})$	$(\frac{h}{2})$	$(\frac{h}{4})$
			R_α/h=2			
3D Ren [26]	2.079	-0.644	3.348	-0.1610	0.0960	0.851
Present 3D	2.079	-0.644	3.347	-0.1609	0.0960	0.851
			R_α/h=4			
3D Ren [26]	0.854	-0.384	2.511	-0.0960	0.0407	0.871
Present 3D	0.854	-0.384	2.511	-0.0960	0.0407	0.871
			R_α/h=10			
3D Ren [26]	0.493	-0.277	2.245	-0.0693	0.0250	0.879
Present 3D	0.493	-0.277	2.245	-0.0693	0.0249	0.879
			R_α/h=50			
3D Ren [26]	0.409	-0.240	2.165	-0.0601	0.0218	0.869
Present 3D	0.409	-0.240	2.165	-0.0601	0.0217	0.869
			R_α/h=100			
3D Ren [26]	0.403	-0.237	2.158	-0.0592	0.0216	0.867
Present 3D	0.403	-0.237	2.158	-0.0592	0.0216	0.867
			R_α/h=500			
3D Ren [26]	0.399	-0.234	2.153	-0.0587	0.0215	0.865
Present 3D	0.399	-0.234	2.152	-0.0585	0.0215	0.864

Table 5: Case 3, present 3D solution compared with the 3D solution proposed by Ren [26] for a composite laminated cylindrical shell.

(α,β)	$\bar{w}$	$\bar{\sigma}_{\alpha\alpha}$	$\bar{\sigma}_{\alpha\alpha}$	$\bar{\sigma}_{\beta\beta}$	$\bar{\sigma}_{\beta\beta}$	$\bar{\sigma}_{\alpha\beta}$	$\bar{\sigma}_{\alpha\beta}$	$\bar{\sigma}_{\beta z}$	$\bar{\sigma}_{\alpha z}$	$\bar{\sigma}_{zz}$
(z)	$(\frac{a}{2},\frac{b}{2})$ (0)	$(\frac{a}{2},\frac{b}{2})$ $(-\frac{h}{2})$	$(\frac{a}{2},\frac{b}{2})$ $(\frac{h}{2})$	$(\frac{a}{2},\frac{b}{2})$ $(-\frac{h}{2})$	$(\frac{a}{2},\frac{b}{2})$ $(\frac{h}{2})$	$(0,0)$ $(-\frac{h}{2})$	$(0,0)$ $(\frac{h}{2})$	$(\frac{a}{2},0)$ $(-\frac{h}{6})$	$(0,\frac{b}{2})$ (0)	$(\frac{b}{2},\frac{b}{2})$ (0)
					R_α/h=2					
3D V&B [27]	10.11	-18.19	7.168	-0.8428	0.1761	-0.2922	0.1797	0.3006	-1.379	-0.34
Present 3D	10.11	-18.19	7.167	-0.8428	0.1761	-0.2922	0.1797	0.3006	-1.379	-0.34
					R_α/h=4					
3D V&B [27]	4.009	-9.323	6.545	-0.2701	0.1270	-0.1609	0.1081	0.1736	-2.349	-0.62
Present 3D	4.009	-9.323	6.544	-0.2701	0.1270	-0.1609	0.1081	0.1736	-2.349	-0.62
					R_α/h=10					
3D V&B [27]	1.223	-5.224	4.683	-0.0791	0.0739	-0.0729	0.0374	0.0826	-3.264	-1.27
Present 3D	1.223	-5.224	4.683	-0.0791	0.0739	-0.0729	0.0374	0.0826	-3.264	-1.27
					R_α/h=50					
3D V&B [27]	0.5495	-3.987	3.930	-0.0225	0.0712	-0.0760	-0.0118	0.0894	-3.491	-4.85
Present 3D	0.5495	-3.986	3.930	-0.0224	0.0712	-0.0760	-0.0118	0.0894	-3.491	-4.85
					R_α/h=100					
3D V&B [27]	0.4715	-3.507	3.507	0.0018	0.0838	-0.1038	-0.0478	0.1223	-3.127	-8.30
Present 3D	0.4715	-3.506	3.507	0.0018	0.0838	-0.1038	-0.0478	0.1223	-3.127	-8.30
					R_α/h=500					
3D V&B [27]	0.1027	-0.7542	0.7895	0.0379	0.0559	-0.0889	-0.0766	0.1051	-0.691	-9.12
Present 3D	0.1027	-0.7543	0.7896	0.0379	0.0559	-0.0889	-0.0766	0.1051	-0.691	-9.12

Table 6: Case 4, present 3D solution compared with the 3D solution proposed by Varadan and Bhaskar [27] for a composite laminated cylinder.

	$\bar{w}(a/2,b/2,0)$							
h/R_α	0.01	0.03	0.05	0.07	0.09	0.1	0.2	0.3
3D Fan & Zhang [45]	0.0541	0.4624	1.1724	2.0863	3.1667	3.7676	12.083	24.706
Present 3D	0.0541	0.4624	1.1723	2.0860	3.1660	3.7664	12.081	24.703

Table 7: Case 5, present 3D solution compared with the 3D solution proposed by Fan and Zhang [45] for a composite laminated spherical panel.

	B1	B2	B3	B4	B5
a[m]	1	1	$2\pi R_\alpha$	$\frac{\pi}{3}R_\alpha$	$\frac{\pi}{3}R_\alpha$
b[m]	1	3	20	20	$\frac{\pi}{3}R_\alpha$
R_α[m]	∞	∞	10	10	10
R_β[m]	∞	∞	∞	∞	10
h_1	h	h/2	h/3	0.1h	h/3
h_2	-	h/2	h/3	0.8h	h/3
h_3	-	-	h/3	0.1h	h/3
sequence	$Iso1$	$Iso1/Iso2$	$Iso1/Iso2/Iso3$	$Iso1/Core/Iso1$	$0°/90°/0°$
$\hat{p}_z$[Pa]	1(top)	1(top)	1(top)	1(top)	1(top)
m[-]	1	1	2	1	1
n[-]	1	1	1	1	1

Table 8: Load and geometrical data for the five proposed new benchmarks.

	Iso1	Iso2	Iso3	Core	Composite
E_1[Pa]	73×10^9	114×10^9	210×10^9	18×10^7	132.38×10^9
E_2[Pa]	73×10^9	114×10^9	210×10^9	18×10^7	10.756×10^9
E_3[Pa]	73×10^9	114×10^9	210×10^9	18×10^7	10.756×10^9
G_{12}[Pa]	$\frac{E}{2(1+\nu)}$	$\frac{E}{2(1+\nu)}$	$\frac{E}{2(1+\nu)}$	$\frac{E}{2(1+\nu)}$	5.6537×10^9
G_{13}[Pa]	$\frac{E}{2(1+\nu)}$	$\frac{E}{2(1+\nu)}$	$\frac{E}{2(1+\nu)}$	$\frac{E}{2(1+\nu)}$	5.6537×10^9
G_{23}[Pa]	$\frac{E}{2(1+\nu)}$	$\frac{E}{2(1+\nu)}$	$\frac{E}{2(1+\nu)}$	$\frac{E}{2(1+\nu)}$	3.603×10^9
ν_{12}	0.3	0.3	0.3	0.37	0.24
ν_{13}	0.3	0.3	0.3	0.37	0.24
ν_{23}	0.3	0.3	0.3	0.37	0.49

Table 9: Material data for the five new benchmark cases proposed in Table 8.

(α,β)	$\bar{u}$ $(0,\frac{b}{2})$	$\bar{v}$ $(\frac{a}{2},0)$	$\bar{w}$ $(\frac{a}{2},\frac{b}{2})$	$\bar{\sigma}_{\alpha\alpha}$ $(\frac{a}{2},\frac{b}{2})$	$\bar{\sigma}_{\beta\beta}$ $(\frac{a}{2},\frac{b}{2})$	$\bar{\sigma}_{\alpha\beta}$ $(0,0)$	$\bar{\sigma}_{zz}$ $(\frac{a}{2},\frac{b}{2})$	$\bar{\sigma}_{\alpha z}$ $(0,\frac{b}{2})$	$\bar{\sigma}_{\beta z}$ $(\frac{a}{2},0)$
					a/h=2				
$z=-h/2$	2.3160	2.3160	4.8277	-0.2079	-0.2079	0.1119	0.0000	0.0000	0.0000
$z=0$	0.5067	0.5067	6.0466	0.0055	0.0055	0.0245	0.4755	0.2277	0.2277
$z=h/2$	-2.1637	-2.1637	7.5963	0.3014	0.3014	-0.1046	1.0000	0.0000	0.0000
					a/h=4				
$z=-h/2$	1.1368	1.1368	3.4463	-0.2041	-0.2041	0.1099	0.0000	0.0000	0.0000
$z=0$	0.0537	0.0537	3.6630	0.0037	0.0037	0.0052	0.4981	0.2362	0.2362
$z=h/2$	-1.0622	-1.0622	3.6237	0.2175	0.2175	-0.1027	1.0000	0.0000	0.0000
					a/h=10				
$z=-h/2$	0.4430	0.4430	2.9120	-0.1988	-0.1988	0.1071	0.0000	0.0000	0.0000
$z=0$	0.0032	0.0032	2.9425	0.0007	0.0007	0.0008	0.4999	0.2383	0.2383
$z=h/2$	-0.4371	-0.4371	2.9166	0.2004	0.2004	-0.1056	1.0000	0.0000	0.0000
					a/h=20				
$z=-h/2$	0.2205	0.2205	2.8302	-0.1979	-0.1979	0.1066	0.0000	0.0000	0.0000
$z=0$	0.0004	0.0004	2.8377	0.0002	0.0002	0.0002	0.5000	0.2386	0.2386
$z=h/2$	-0.2197	-0.2197	2.8305	0.1983	0.1983	-0.1062	1.0000	0.0000	0.0000
					a/h=50				
$z=-h/2$	0.0881	0.0881	2.8070	-0.1976	-0.1976	0.1064	0.0000	0.0000	0.0000
$z=0$	0.0000	0.0000	2.8082	0.0000	0.0000	0.0000	0.5000	0.2387	0.2387
$z=h/2$	-0.0880	-0.0880	2.8070	0.1977	0.1977	-0.1063	1.0000	0.0000	0.0000
					a/h=100				
$z=-h/2$	0.0440	0.0440	2.8037	-0.1976	-0.1976	0.1064	0.0000	0.0000	0.0000
$z=0$	0.0000	0.0000	2.8040	0.0000	0.0000	0.0000	0.5000	0.2387	0.2387
$z=h/2$	-0.0440	-0.0440	2.8037	0.1976	0.1976	-0.1064	1.0000	0.0000	0.0000

Table 10: Benchmark 1, 3D exact results for displacements and stresses in an isotropic one-layered square plate.

(α,β)	$\bar{u}$ $(0,\frac{b}{2})$	$\bar{v}$ $(\frac{a}{2},0)$	$\bar{w}$ $(\frac{a}{2},\frac{b}{2})$	$\bar{\sigma}_{\alpha\alpha}$ $(\frac{a}{2},\frac{b}{2})$	$\bar{\sigma}_{\beta\beta}$ $(\frac{a}{2},\frac{b}{2})$	$\bar{\sigma}_{\alpha\beta}$ $(0,0)$	$\bar{\sigma}_{zz}$ $(\frac{a}{2},\frac{b}{2})$	$\bar{\sigma}_{\alpha z}$ $(0,\frac{b}{2})$	$\bar{\sigma}_{\beta z}$ $(\frac{a}{2},0)$
					a/h=2				
$z=-h/2$	6.5035	2.1678	10.690	-0.4640	-0.1846	0.1048	0.0000	0.0000	0.0000
$z=0^*$	1.5677	0.5226	12.427	-0.0637	0.0037	0.0253	0.4498	0.4065	0.1355
$z=h/2$	-5.2585	-1.7528	13.043	0.6930	0.3402	-0.1323	1.0000	0.0000	0.0000
					a/h=4				
$z=-h/2$	3.2336	1.0778	8.3065	-0.4614	-0.1836	0.1042	0.0000	0.0000	0.0000
$z=0^*$	0.4304	0.1435	8.6631	-0.0489	-0.0119	0.0139	0.4671	0.4200	0.1400
$z=h/2$	-2.5676	-0.8559	8.5448	0.5990	0.2544	-0.1292	1.0000	0.0000	0.0000
					a/h=10				
$z=-h/2$	1.2841	0.4280	7.5124	-0.4581	-0.1822	0.1034	0.0000	0.0000	0.0000
$z=0^*$	0.1338	0.0446	7.5658	-0.0457	-0.0170	0.0108	0.4709	0.4237	0.1412
$z=h/2$	-1.0280	-0.3427	7.5344	0.5770	0.2321	-0.1293	1.0000	0.0000	0.0000
					a/h=20				
$z=-h/2$	0.6412	0.2137	7.3943	-0.4575	-0.1820	0.1033	0.0000	0.0000	0.0000
$z=0^*$	0.0642	0.0214	7.4075	-0.0453	-0.0177	0.0103	0.4714	0.4242	0.1414
$z=h/2$	-0.5142	-0.1714	7.3993	0.5740	0.2290	-0.1294	1.0000	0.0000	0.0000
					a/h=50				
$z=-h/2$	0.2564	0.0855	7.3611	-0.4573	-0.1819	0.1033	0.0000	0.0000	0.0000
$z=0^*$	0.0254	0.0085	7.3632	-0.0452	-0.0179	0.0102	0.4715	0.4243	0.1414
$z=h/2$	-0.2057	-0.0686	7.3618	0.5732	0.2281	-0.1294	1.0000	0.0000	0.0000
					a/h=100				
$z=-h/2$	0.1282	0.0427	7.3563	-0.4573	-0.1819	0.1033	0.0000	0.0000	0.0000
$z=0^*$	0.0127	0.0042	7.3568	-0.0452	-0.0180	0.0102	0.4716	0.4243	0.1414
$z=h/2$	-0.1029	-0.0343	7.3565	0.5731	0.2280	-0.1294	1.0000	0.0000	0.0000

Table 11: Benchmark 2, 3D exact results for displacements and stresses in an isotropic two-layered rectangular plate. * top of the first layer.

(α,β)	$\bar{u}$ $(0,\frac{b}{2})$	$\bar{v}$ $(\frac{a}{2},0)$	$\bar{w}$ $(\frac{a}{2},\frac{b}{2})$	$\bar{\sigma}_{\alpha\alpha}$ $(\frac{a}{2},\frac{b}{2})$	$\bar{\sigma}_{\beta\beta}$ $(\frac{a}{2},\frac{b}{2})$	$\bar{\sigma}_{\alpha\beta}$ $(0,0)$	$\bar{\sigma}_{zz}$ $(\frac{a}{2},\frac{b}{2})$	$\bar{\sigma}_{\alpha z}$ $(0,\frac{b}{2})$	$\bar{\sigma}_{\beta z}$ $(\frac{a}{2},0)$
					R_α/h=2				
$z=-h/2$	1663.7	1058.4	2555.1	151.60	-287.03	309.58	0.0000	0.0000	0.0000
$z=0$	1422.3	236.60	2563.8	393.06	29.521	296.81	0.3691	59.521	227.99
$z=h/2$	1182.6	-624.15	2482.0	950.33	924.17	300.56	1.0000	0.0000	0.0000
					R_α/h=4				
$z=-h/2$	422.85	150.89	704.47	110.22	-61.742	128.72	0.0000	0.0000	0.0000
$z=0$	385.27	20.358	696.31	215.99	51.163	150.29	0.3382	20.042	72.145
$z=h/2$	348.82	-109.58	680.18	464.52	356.17	199.39	1.0000	0.0000	0.0000
					R_α/h=10				
$z=-h/2$	64.579	7.7543	112.96	51.954	3.4058	42.155	0.0000	0.0000	0.0000
$z=0$	62.078	-1.0074	112.04	87.967	29.850	57.963	0.3296	3.4264	12.216
$z=h/2$	59.623	-9.7050	110.90	173.11	98.787	93.397	1.0000	0.0000	0.0000
					R_α/h=50				
$z=-h/2$	2.4569	-0.0584	4.4011	10.941	3.7410	7.3083	0.0000	0.0000	0.0000
$z=0$	2.4373	-0.1274	4.3921	17.345	6.8057	11.115	0.3278	0.1350	0.4846
$z=h/2$	2.4178	-0.1963	4.3828	32.386	14.271	19.935	1.0000	0.0000	0.0000
					R_α/h=100				
$z=-h/2$	0.6096	-0.0258	1.0950	5.4948	2.0543	3.5830	0.0000	0.0000	0.0000
$z=0$	0.6072	-0.0344	1.0939	8.6448	3.4480	5.5215	0.3276	0.0336	0.1208
$z=h/2$	0.6047	-0.0430	1.0927	16.033	6.7839	10.036	1.0000	0.0000	0.0000
					R_α/h=500				
$z=-h/2$	0.0242	-0.0014	0.0436	1.1024	0.4399	0.7052	0.0000	0.0000	0.0000
$z=0$	0.0242	-0.0015	0.0436	1.7242	0.6966	1.0984	0.3275	0.0013	0.0048
$z=h/2$	0.0242	-0.0015	0.0436	3.1804	1.3004	2.0179	1.0000	0.0000	0.0000

Table 12: Benchmark 3, 3D exact results for displacements and stresses in an isotropic three-layered cylinder.

	$\bar{u}$	$\bar{v}$	$\bar{w}$	$\bar{\sigma}_{\alpha\alpha}$	$\bar{\sigma}_{\beta\beta}$	$\bar{\sigma}_{\alpha\beta}$	$\bar{\sigma}_{zz}$	$\bar{\sigma}_{\alpha z}$	$\bar{\sigma}_{\beta z}$
(α,β)	$(0, \frac{b}{2})$	$(\frac{a}{2}, 0)$	$(\frac{a}{2}, \frac{b}{2})$	$(\frac{a}{2}, \frac{b}{2})$	$(\frac{a}{2}, \frac{b}{2})$	$(0, 0)$	$(\frac{a}{2}, \frac{b}{2})$	$(0, \frac{b}{2})$	$(\frac{a}{2}, 0)$
					R_α/h=2				
$z = -h/2$	40266	-4978.0	93446	-7499.4	-685.94	3333.6	0.0000	0.0000	0.0000
$z = 0$	66015	2201.2	119525	22.675	49.695	19.852	0.4650	134.84	71.574
$z = h/2$	41975	-20864	155004	7380.9	8843.8	1220.0	1.0000	0.0000	0.0000
					R_α/h=4				
$z = -h/2$	13575	-2582.2	35367	-2157.2	975.29	1918.6	0.0000	0.0000	0.0000
$z = 0$	13196	-2931.9	35910	10.784	16.748	4.2956	0.3553	153.28	87.943
$z = h/2$	11031	-4558.4	37396	2652.7	3678.7	795.59	1.0000	0.0000	0.0000
					R_α/h=10				
$z = -h/2$	2295.8	-493.71	6250.2	-481.25	631.15	787.34	0.0000	0.0000	0.0000
$z = 0$	2101.5	-607.44	6228.5	1.4602	3.3141	1.3307	0.1138	141.56	82.857
$z = h/2$	1892.5	-737.02	6220.3	953.96	1446.9	333.46	1.0000	0.0000	0.0000
					R_α/h=50				
$z = -h/2$	132.14	-31.609	370.29	-63.159	229.31	214.96	0.0000	0.0000	0.0000
$z = 0$	123.90	-36.515	370.04	0.2456	0.7768	0.3828	-0.1433	45.791	25.478
$z = h/2$	115.67	-41.423	369.63	230.51	394.61	112.79	1.0000	0.0000	0.0000
					R_α/h=100				
$z = -h/2$	35.615	-9.3410	102.52	0.5634	146.90	106.85	0.0000	0.0000	0.0000
$z = 0$	34.315	-10.110	102.48	0.1596	0.4538	0.2121	0.0853	14.734	8.1505
$z = h/2$	33.015	-10.878	102.43	93.426	198.93	74.566	1.0000	0.0000	0.0000
					R_α/h=500				
$z = -h/2$	1.4420	-0.4148	4.2730	7.8247	34.923	19.607	0.0000	0.0000	0.0000
$z = 0$	1.4306	-0.4215	4.2727	0.0332	0.0945	0.0442	0.4088	0.6476	0.3576
$z = h/2$	1.4193	-0.4282	4.2723	11.883	37.194	18.196	1.0000	0.0000	0.0000

Table 13: Benchmark 4, 3D exact results for displacements and stresses in a sandwich cylindrical shell.

	$\bar{u}$	$\bar{v}$	$\bar{w}$	$\bar{\sigma}_{\alpha\alpha}$	$\bar{\sigma}_{\beta\beta}$	$\bar{\sigma}_{\alpha\beta}$	$\bar{\sigma}_{zz}$	$\bar{\sigma}_{\alpha z}$	$\bar{\sigma}_{\beta z}$
(α,β)	$(0,\frac{b}{2})$	$(\frac{a}{2},0)$	$(\frac{a}{2},\frac{b}{2})$	$(\frac{a}{2},\frac{b}{2})$	$(\frac{a}{2},\frac{b}{2})$	$(0,0)$	$(\frac{a}{2},\frac{b}{2})$	$(0,\frac{b}{2})$	$(\frac{a}{2},0)$
					R_α/h=2				
$z=-h/2$	277.82	354.49	566.75	-911.37	-150.23	265.89	0.0000	0.0000	0.0000
$z=0$	228.52	205.02	632.22	49.720	82.980	136.73	0.4798	285.34	272.89
$z=h/2$	128.55	-50.872	770.96	887.79	287.58	19.598	1.0000	0.0000	0.0000
					R_α/h=4				
$z=-h/2$	87.222	99.941	185.49	-443.19	-60.907	134.92	0.0000	0.0000	0.0000
$z=0$	58.281	54.432	188.49	14.791	130.89	71.095	0.2214	252.15	141.27
$z=h/2$	30.897	0.0726	190.23	467.56	107.30	17.364	1.0000	0.0000	0.0000
					R_α/h=10				
$z=-h/2$	18.116	17.599	43.854	-138.87	-12.122	59.283	0.0000	0.0000	0.0000
$z=0$	13.214	12.079	43.886	6.4550	95.841	39.885	0.0697	128.11	44.096
$z=h/2$	8.4961	6.2081	43.511	221.56	32.922	22.083	1.0000	0.0000	0.0000
					R_α/h=50				
$z=-h/2$	0.7249	0.6644	2.2184	3.0086	1.1961	11.064	0.0000	0.0000	0.0000
$z=0$	0.6654	0.6044	2.2165	1.6645	25.247	10.012	0.3583	8.2353	2.4247
$z=h/2$	0.6063	0.5437	2.2135	24.988	3.5657	8.9781	1.0000	0.0000	0.0000
					R_α/h=100				
$z=-h/2$	0.1746	0.1592	0.5570	4.3260	0.8807	5.2904	0.0000	0.0000	0.0000
$z=0$	0.1671	0.1517	0.5567	0.8241	12.718	5.0262	0.4282	2.0851	0.6106
$z=h/2$	0.1596	0.1441	0.5563	9.8812	1.4767	4.7644	1.0000	0.0000	0.0000
					R_α/h=500				
$z=-h/2$	0.0067	0.0061	0.0222	1.3108	0.2201	1.0123	0.0000	0.0000	0.0000
$z=0$	0.0067	0.0060	0.0222	0.1615	2.5414	1.0018	0.4857	0.0833	0.0244
$z=h/2$	0.0066	0.0060	0.0222	1.5327	0.2439	0.9913	1.0000	0.0000	0.0000

Table 14: Benchmark 5, 3D exact results for displacements and stresses in a three-layered laminated composite spherical shell.

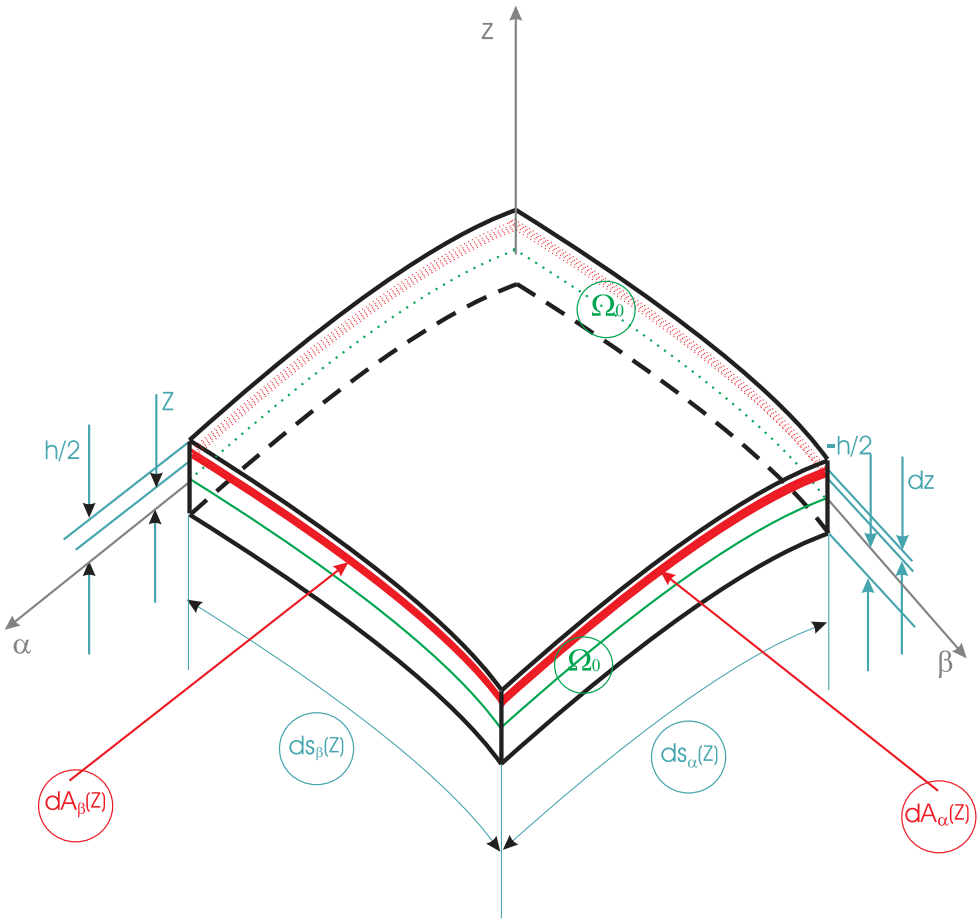

Figure 1: Geometrical data, parameters and notations for the proposed 3D shell formulation.

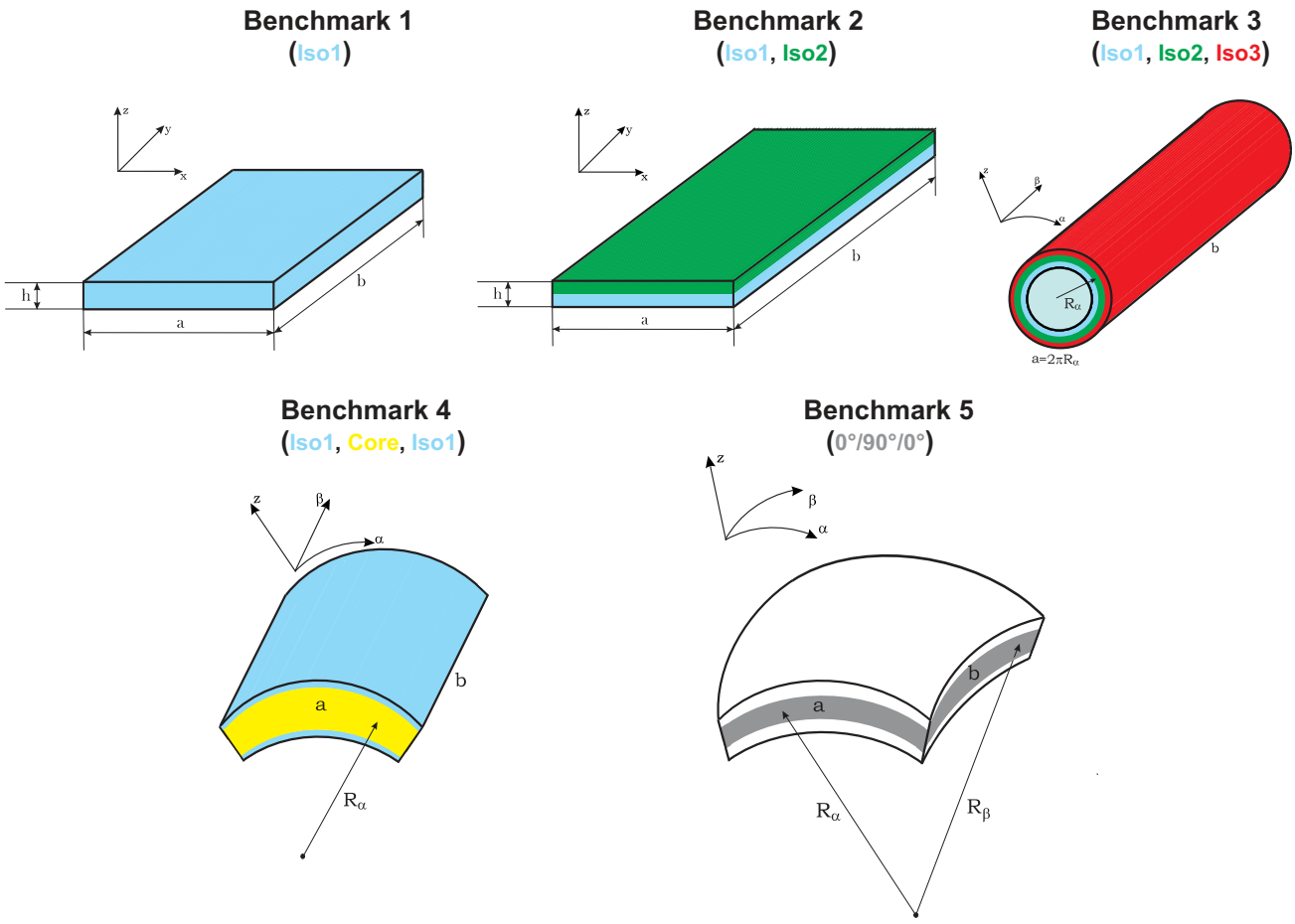

Figure 2: Geometries and reference systems for the five proposed new benchmarks.

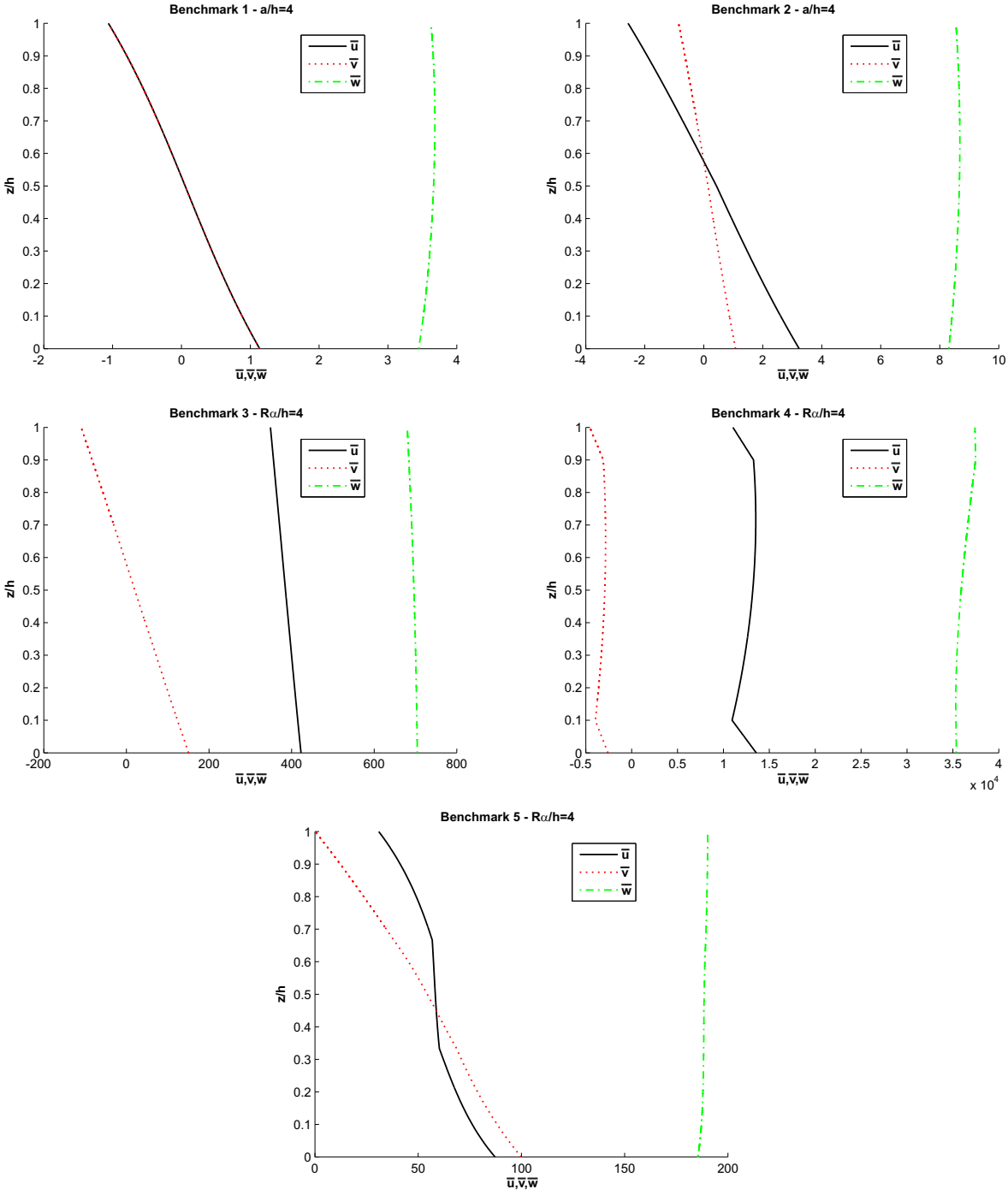

Figure 3: No-dimensional displacement components through the thickness direction for the five proposed new benchmarks.

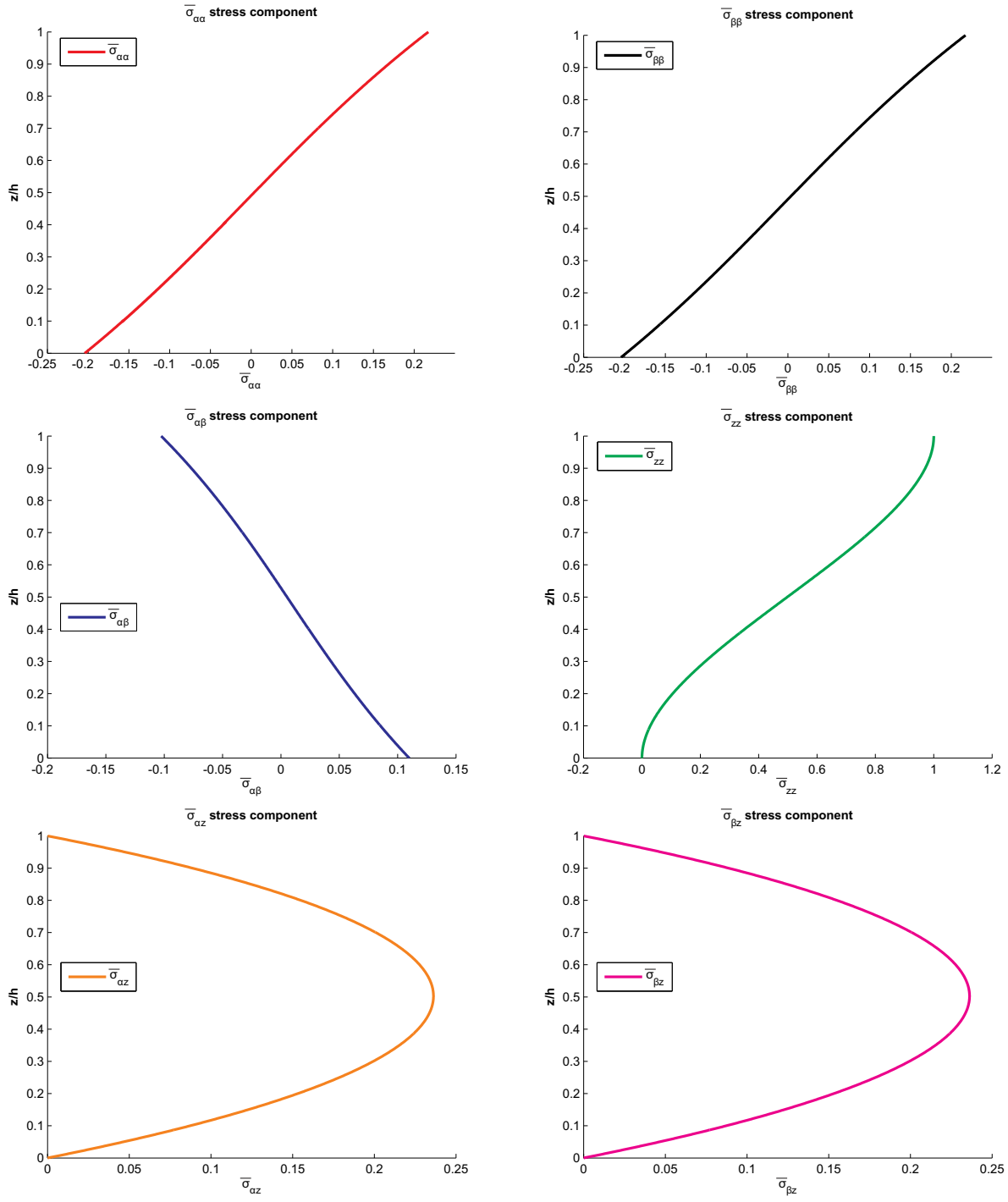

Figure 4: No-dimensional stress components through the thickness direction for the benchmark 1 about the isotropic one-layered square plate with a/h=4.

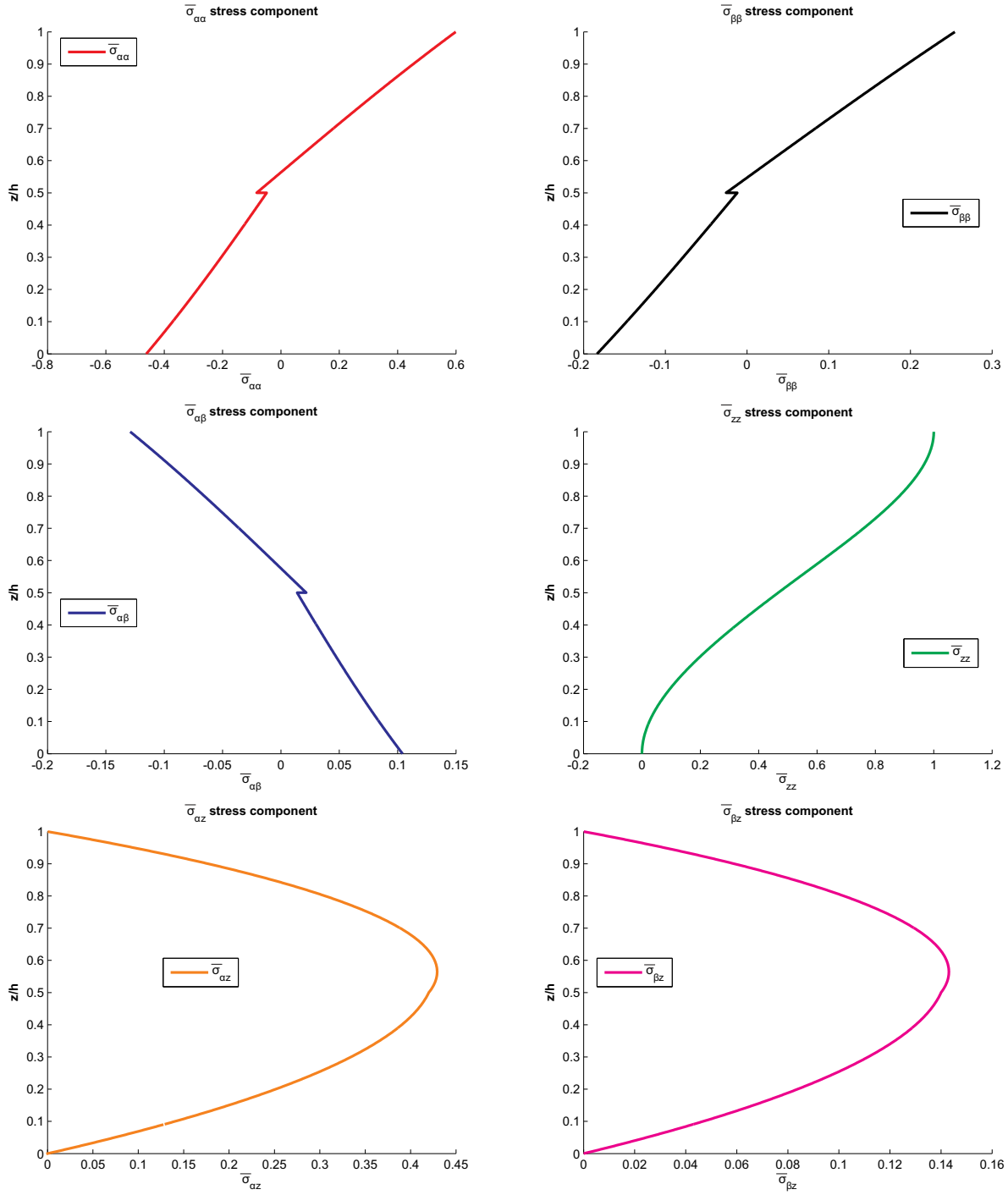

Figure 5: No-dimensional stress components through the thickness direction for the benchmark 2 about the isotropic two-layered rectangular plate with a/h=4.

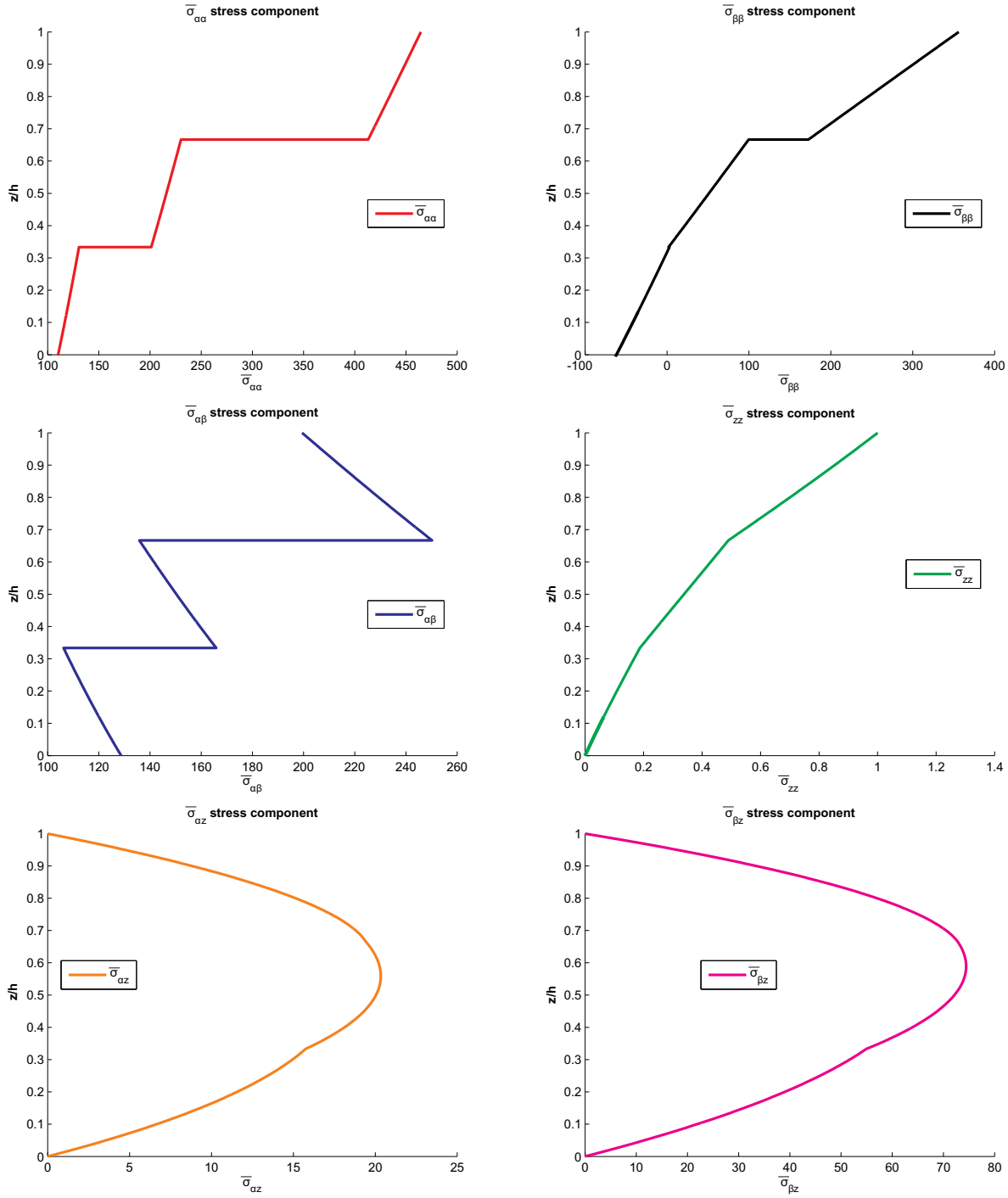

Figure 6: No-dimensional stress components through the thickness direction for the benchmark 3 about the isotropic three-layered cylinder with R_α/h=4.

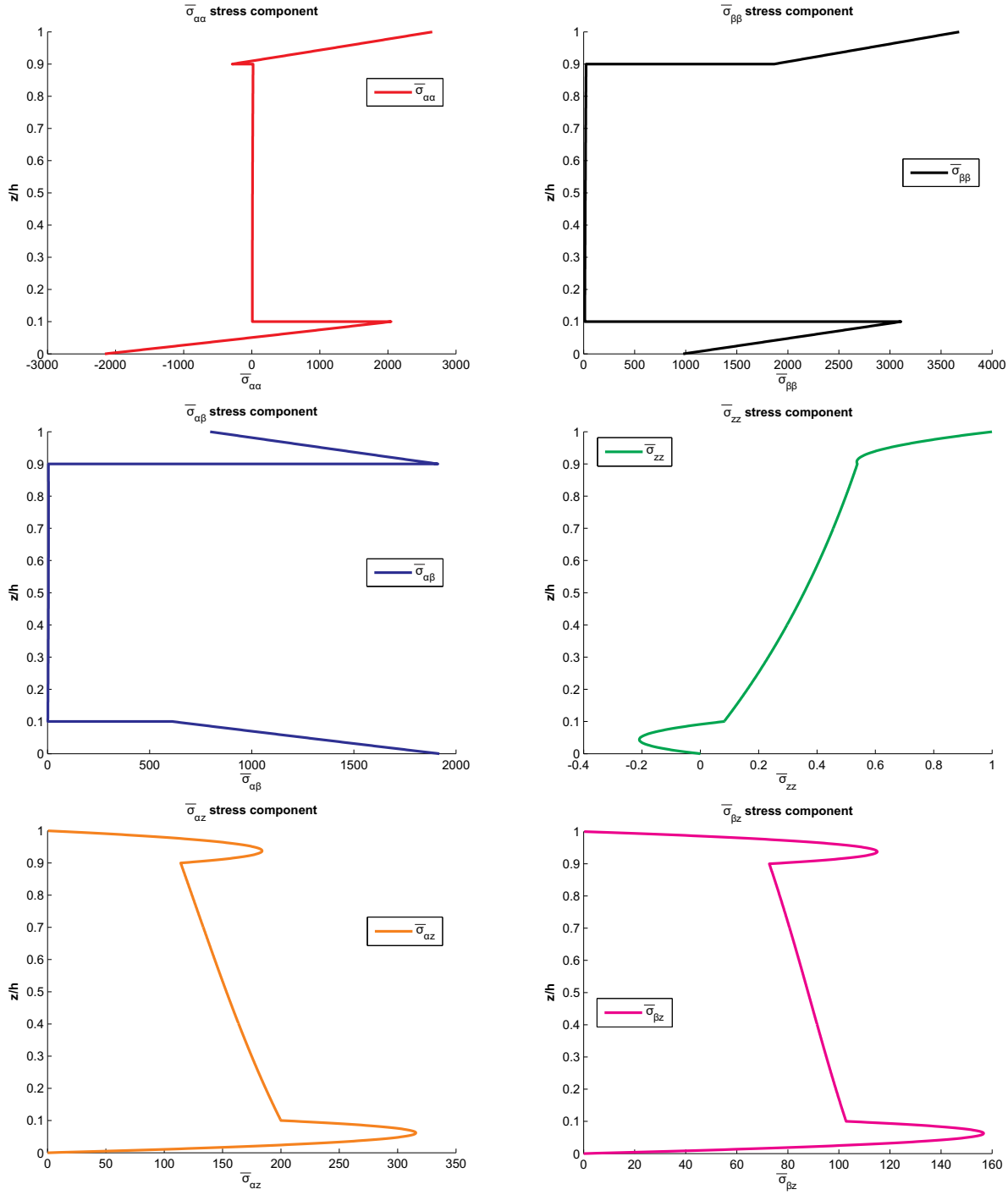

Figure 7: No-dimensional stress components through the thickness direction for the benchmark 4 about the sandwich cylindrical shell panel with R_α/h=4.

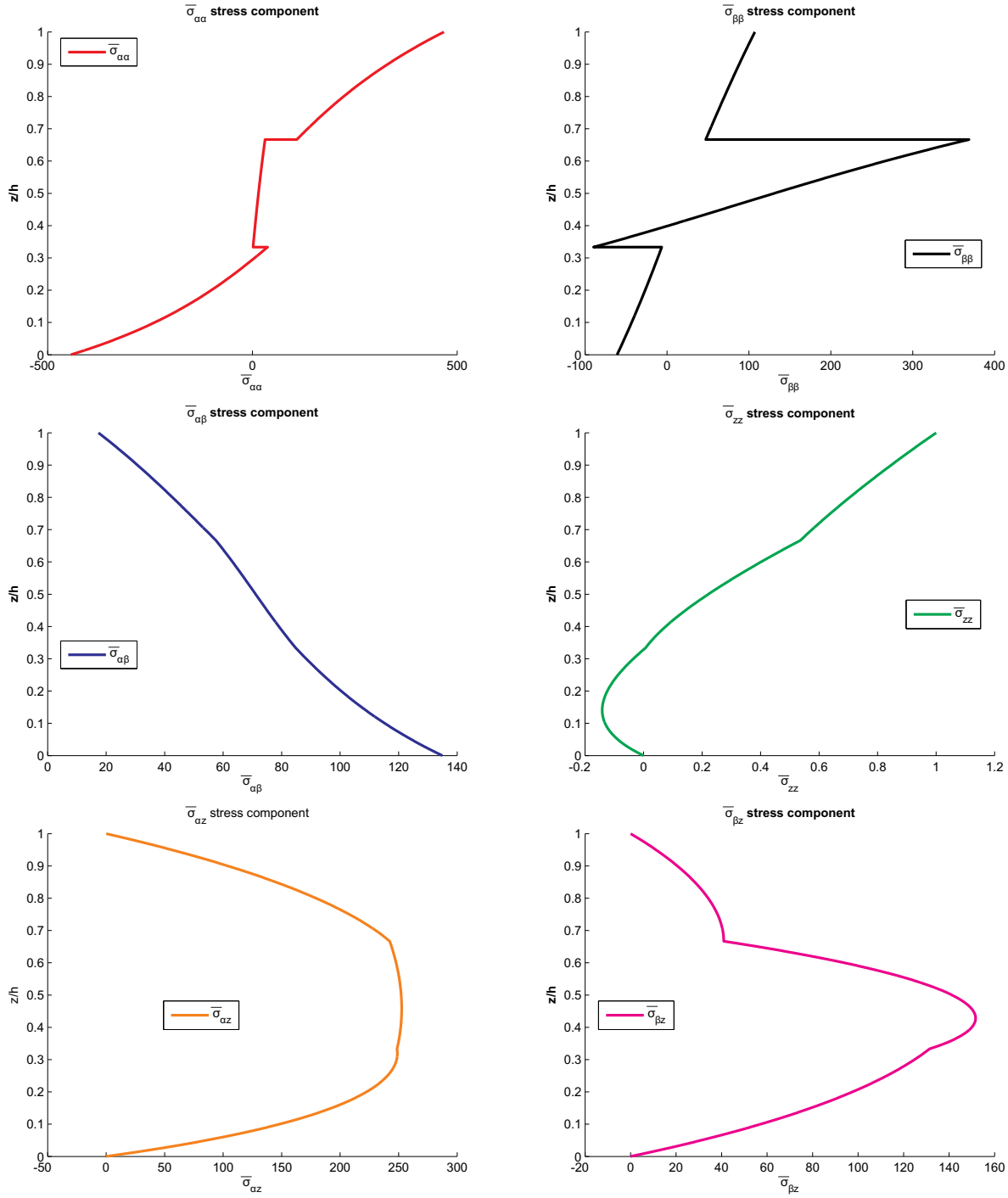

Figure 8: No-dimensional stress components through the thickness direction for the benchmark 5 about the composite spherical shell panel with R_α/h=4.